DEVELOPMENT OF A FIBER OPTIC TORQUE SENSOR AND A SINGLE CHANNEL, HIGH PRECISION OPTICAL STRAIN MEASUREMENT PLATFORM

by

Nicholas Burgwin

Bachelor of Applied Science

University of Toronto, 2010

A thesis presented to Ryerson University

in partial fulfillment of the

requirements for the degree of

Master of Applied Science

in the Program of

Electrical and Computer Engineering

Toronto, Ontario, Canada, 2016

Author's Declaration

I hereby declare that I am the sole author of this thesis. This is a true copy of the thesis, including any required final revisions, as accepted by my examiners.

I authorize Ryerson University to lend this thesis to other institutions or individuals for the purpose of scholarly research.

I further authorize Ryerson University to reproduce this thesis by photocopying or by other means, in total or in part, at the request of other institutions or individuals for the purpose of scholarly research.

I understand that my thesis may be made electronically available to the public.

Abstract

DEVELOPMENT OF A FIBER OPTIC TORQUE SENSOR AND A SINGLE CHANNEL, HIGH PRECISION OPTICAL STRAIN MEASUREMENT PLATFORM

Nicholas Burgwin
Ryerson University - Electrical and Computer Engineering
Master of Applied Science – 2016

Fiber optic sensors based on Fiber Bragg Grating (FBG) technology have been successfully adopted for sensor measurements for almost two decades. The advantages offered by FBG sensors, such as Electro-Magnetic Interference immunity and inherent intrinsic safety, provide motivation for the development of a commercial measurement platform. With the development of an FBG Fabry-Perot cavity, a sensor with sub-picometer spectral width allows for a factor of 1000 times improvement in strain measurement.

This thesis presents the development of a highly-accurate optical measurement platform based on the FBG Fabry-Perot cavity and Pound-Drever-Hall (PDH) laser locking technique that is demonstrated through the development of an optical torque sensor. With the fiber optic sensor designed as per the PDH requirements, the platform achieved a measurement accuracy of +/- 0.015% of the full-scale torque value of 188N·m. With the platform at ~$2,000, a successful demonstration of the platform and a fiber optic torque sensor is presented.

Acknowledgements

I would like to express my appreciation and gratitude towards my supervising professor, Dr. Xijia Gu, who helped guide me through this research and challenged me to continually improve in my work. He has been a tremendous resource with helping overcome technical challenges as well as practical, real-world challenges. From our lab, I would like to thank Jiang Li for the amazing work she does in producing the fiber optic sensors used throughout my research activities.

I would like to thank Dr. Hua Lu for providing me access to his mechanical engineering lab, and in being a committee member for my defense along with Dr. Mahmood Kassam. Both offered excellent feedback that is not limited to improvements in this work, but can be utilized in future work as well. From the mechanical engineering department, I would like to thank Chao Ma for the assistance offered in setting up and running the torsion test machine heavily utilized throughout this work.

Finally, I would like to thank my family for the support throughout my time at Ryerson.

Dedication

This work is dedicated to the memory of my mother, Joan Burgwin, for her continual support of my pursuit of learning and finding intellectual challenges. Although this pursuit may not always be practical or logical, I hope I never lose the passion for learning as she never did.

Table of Contents

List of Tables

List of Figures

1. Introduction

As the world begins to see larger electrification and the cost of integrating electronics reduces, sensors are being integrated more often to actively monitor for safety and improve performance and reliability of products during both manufacturing and operation. With the increased adoption of electric vehicles and renewable energies, such as wind turbines, the need to monitor torque accurately in rotating parts is increasing in demand. Globally, the market for torque sensors was estimated to be worth $1.1 Billion USD in 2015 and is anticipated to reach $1.9 Billion USD by 2021 [1]. Applications of torque monitoring exist across a variety of different industries, with a variety of different design constraints and considerations. To name a few, torque sensors are seeing adoption in the medical industry in prosthetic limbs, in automotive applications for monitoring torque from electric motors, and in manufacturing through use in torque screwdrivers and verification tools [2].

The measurement technology most often used in torque sensors commercially available today is a foil strain gauge; a technology that has remained almost unchanged since its invention in the early 1950's [3]. Although it is a well-known and used technology, limitations due to electromagnetic interference susceptibility, lack of inherent intrinsic safety and degradation over time requiring re-calibration do still exist [4].

Fiber optic sensors have begun to see commercial adoption over the last decade, with a number of commercially available sensors and measurement platforms being offered by competing companies. Adoption has been limited due to cost compared to conventional technologies, such as strain gauge based electrical sensors, and as a result the technology has only seen success in Civil, Oil and Gas, and Aerospace industries [5]. In this work, a fiber optic sensor and a high precision, low cost optical measurement platform based off the Pound-Drever-Hall (PDH) technique is demonstrated by measuring torque applied to an aluminum torsion rod and the measurement performance is compared against foil strain gauge measurements.

1.1   Foil Strain Gauge Technology

A foil strain gauge is a precision resistor that is bonded onto a component that is exposed to a mechanical force which causes a deformation; this is known as strain. Due to the applied strain

on the material, and therefore to the strain gauge through the bond, the strain gauge will deform and cause a change in length, and therefore a change in resistance. The gauge factor, GF, of a foil strain gauge is the ratio of relative change in electrical resistance to the mechanical strain, which is typically 2-5 [6]. With a gauge factor of 2, and a nominal resistance of 350Ω, the change in resistance of the strain gauge would be 0.7mΩ/$\mu\varepsilon$. In order to monitor this small change, the strain gauge is often used within a Wheatstone bridge configuration, as seen in Figure 1 [6].
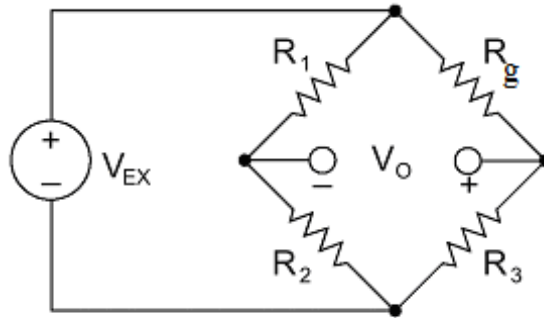
Figure 1 - Wheatstone bridge

In this configuration, the nominal resistance of R_1, R_2, R_3 and R_g are all equal when unstrained, and the output at V_o is zero. As R_g experiences strain, the resistance of R_g will change, and so will the output at V_o. This change is typically in millivolts, as the change in resistance is small, and commonly the output of the Wheatstone bridge is amplified. This configuration also allows for temperature compensation, as the three other resistances can be located near R_g and would therefore see a similar change in resistance due to a temperature change.

1.2 Foil Strain Gauge Benefits and Limitations

Foil strain gauges are well known devices after decades of use and development, and as a result are easy to manufacturer. In addition, they are very easy to use as the principle of operation is simple to understand and with the ubiquity of electronic equipment, easy to monitor. The dimensions of the strain gauge are also very flexible, allowing for them to be bonded to small components.

The limitations of the foil strain gauges, however, can often prevent measurements being performed. As they are metal, they are susceptible to electromagnetic interference (EMI); electrical radiation emitted from other electrical devices. Due to the small resistance change due to strain, and the small voltage signal that is used to monitor this change, electrical noise can

mask or entirely prevent small strain measurements from being performed [4]. Although new techniques have been presented and are being used in industry, such as AC excitation of the bridge rather than DC excitation, there will always be an influence due to EMI in high areas of radiation, such as in a power station transformer or within an electric motor. This can therefore prevent measurements from being performed in particular locations due to the sensors susceptibility to picking up EMI. For vibrational measurements, the mass of the gauge, wiring and bonding material (i.e. epoxy) can also mask or influence the specimen under test; something often overlooked and hard to isolate.

Error can also occur over-time as the strain gauge material begins to relax and deform due to rapid strain impacts; known as strain-gauge creep. This issue is a material problem which can be improved by better selection of the foil strain gauge material and the bonding agent being used, but is still a limitation of the construction of the foil strain gauge.

1.3   Foil Strain Gauge Torque Sensors

Torque sensors used for monitoring rotating equipment are commonly installed in the path between the drive and the device under test and are referred to as in-line torque sensors. As can be seen in Figure 2, the torque sensor is connected to the output of the drive through a coupler, and on the other side, is connected to the device under test through another coupler. These couplers are required in order to protect the transducer from bending forces that exist due to misalignment within the mechanical fixture. These couplers are commonly made from hard, yet elastic rubber, allowing for misalignment to be compensated for while being stiff enough to transmit the applied torque. These couplers add rotational inertia to the system and dampen response to dynamic torque vibrations that could be present in the device under test. In addition
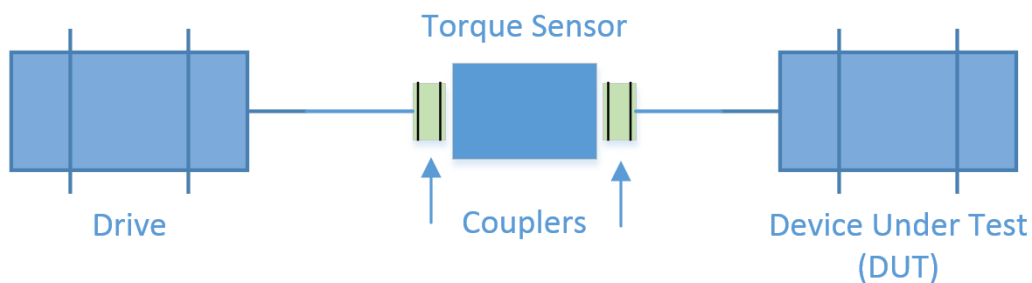
Figure 2 - In-line Torque sensor between the drive and the device under test

3
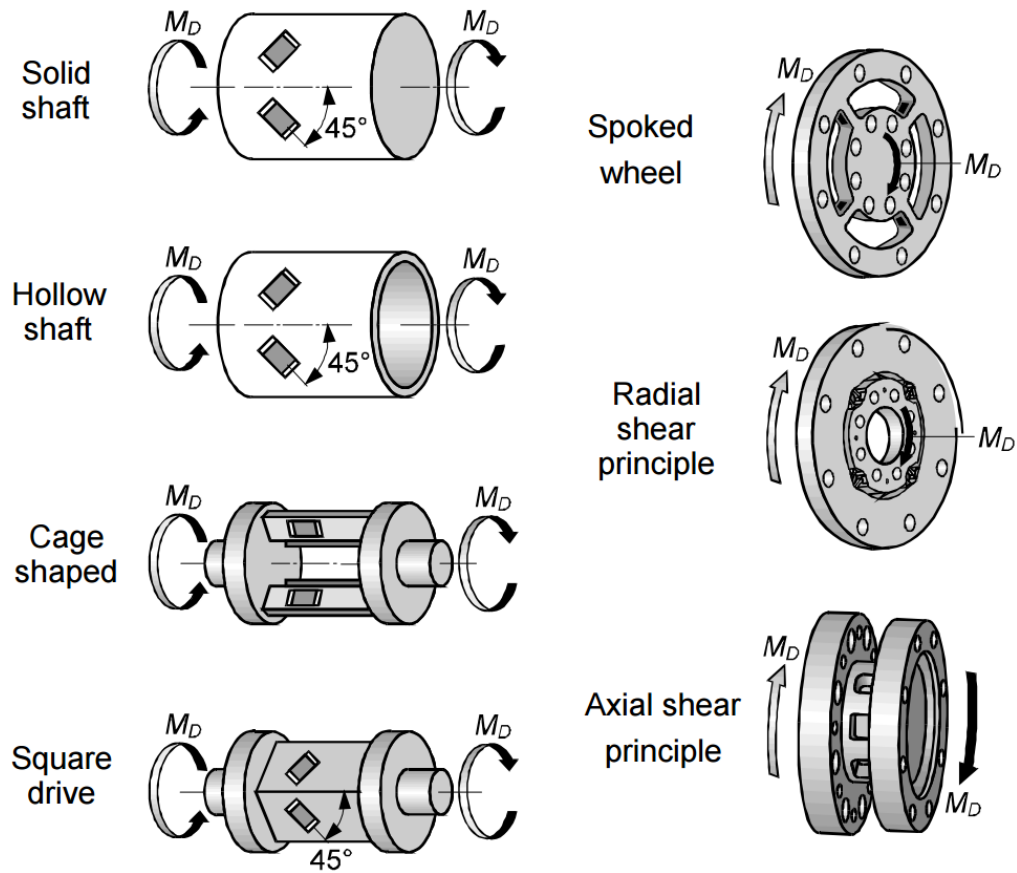
Figure 3 - Common in-line torque sensor body configurations and strain gauge bonding locations [18].

to masking potentially important information, they add system cost and complexity.

There are a variety of different configurations in which strain gauges are bonded internally within the in-line torque transducer, as can be seen in Figure 3.

The different geometries presented exist to allow for improved torque measurements in varying applications. For high torque measurement ranges, the square drive is often used, but for applications that require higher bending stiffness, a tubular body is preferred. Thin flanges, in comparison, allow for improved accuracy at low torque values, as the flexural stiffness is significantly improved upon.

Although there are a number of manufacturers for torque sensors, HBM is one of the industry's largest suppliers with some of the most accurate sensors commercially available. The T12, a flange based torque transducer as seen in Figure 4, has a measurement resolution of +/- 0.05% of

Figure 4 - HBM T12 Flange Torque Transducer [7].

full-scale (FS) torque, which can be as low as 100 N·m and as high as 10 kN·m at a measurement frequency up to 6 kHz [7].

Although offering excellent performance, mechanical mounting limitations still exist with this device which can impact torque measurements. The T12 still requires that two couplers, made of hard rubber material, are used to mount the device in-line. With the need to include these couplers, the possibility of losing torque data due to the rubber isolating torque will exist.

1.4   Fiber Optic Sensors

Fiber Bragg Gratings (FBG's) were a Canadian invention first demonstrated by Dr. Kenneth Hill in 1978 at the Communications Research Centre (CRC) [8]. FBG sensors have since seen adoption from the early 2000's in Civil, Oil & Gas and Aerospace for strain monitoring.

The working principle of an FBG is well known today as is the manufacturing technique and will be briefly reviewed to aid the readers understanding. An FBG is formed in the core of a photosensitive single-mode fiber by changing the refractive index periodically over a certain length of the fiber. The periodic grating that is formed will reflect light of the same wavelength, defined as the Bragg wavelength, λ_B, in equation (1).

$$\lambda_B = 2n_e\Lambda \tag{1}$$
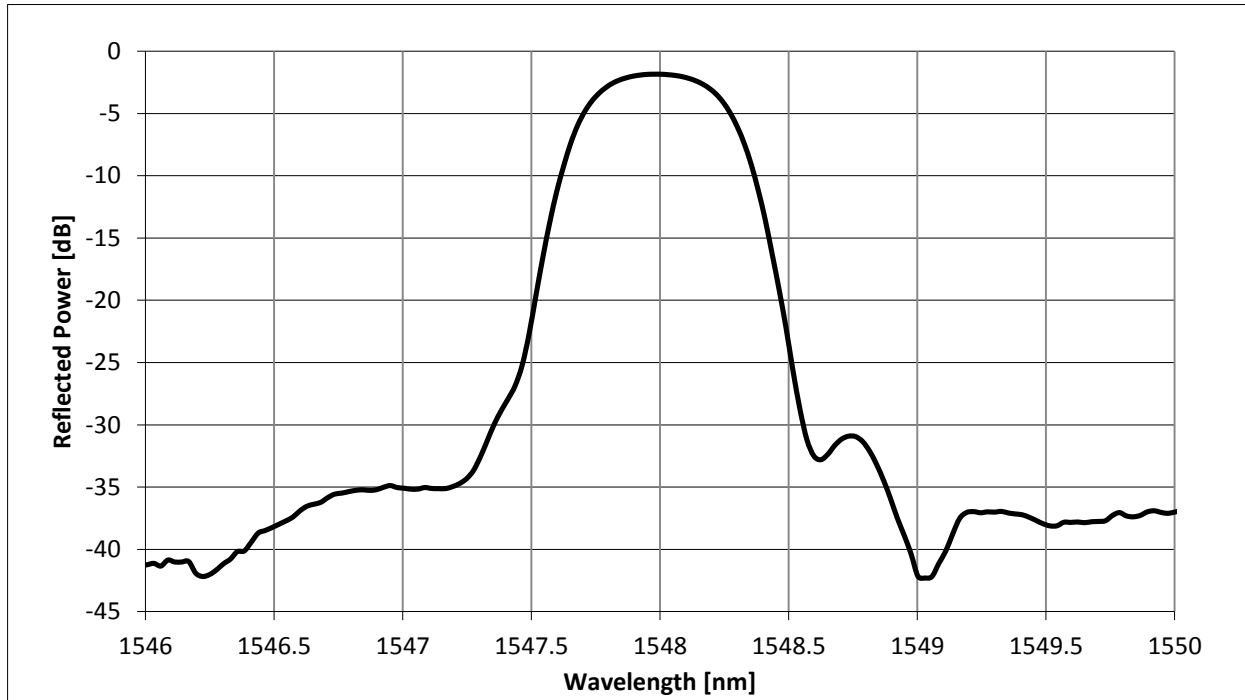
Figure 5 - Typical FBG manufactured using UV manufacturing process; λ_B = 1548.0nm
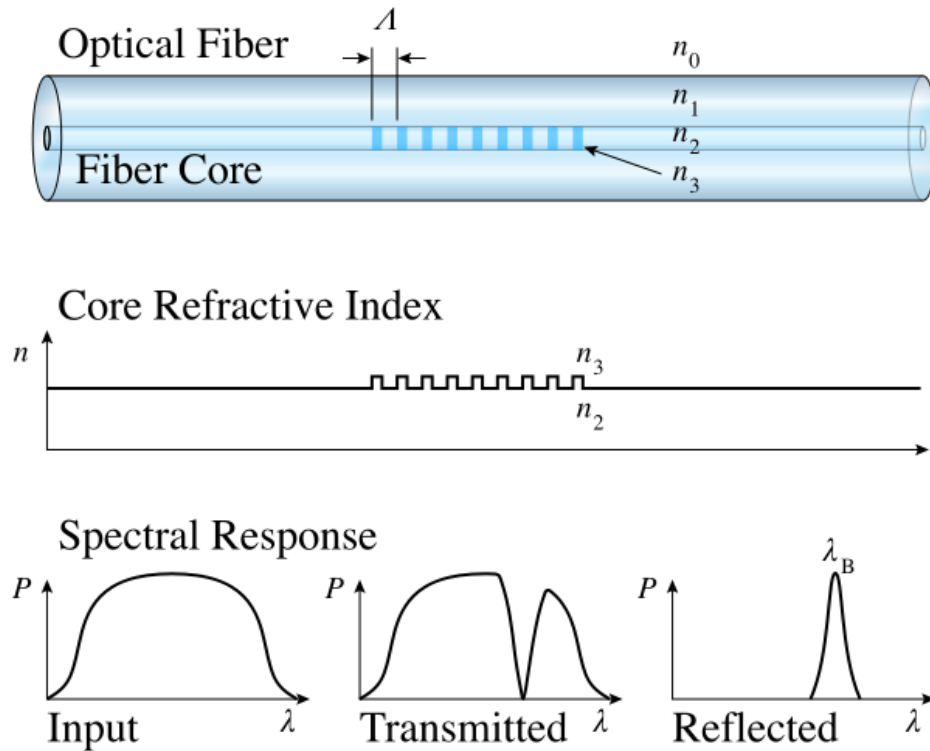
Figure 6 - Fiber Bragg Grating manufactured inside the core of the single-mode fiber through periodic refractive index changes. The spectral response shows the FBG reflects a particular portion of the input light, known as the Bragg wavelength. Photo by Sakurambo is licensed under CC BY 2.0

6

where n_e is the effective reflective index of the grating in the fiber, and Λ is the grating period. A FBGs reflection spectrum, manufactured with a $\lambda_B = 1548.0$nm and a spectral width of approximately 0.6nm, can be seen in Figure 5. As can be imagined, by reviewing Figure 6, if we apply axial strain to the fiber where there FBG is located, we can change the grating period. This strain can either be due to tension or compression, as either will result in a change of length, and therefore a measurable strain, ε, as seen in equation (2).

$$\varepsilon = {\Delta L}/{L} \tag{2}$$

As the applied strain causes a change in the grating period, a shift in the Bragg wavelength will occur, and therefore the wavelength of light reflected from the FBG will shift as well, as shown in equation (3).

$$\Delta\lambda = \lambda_o * (1 - \rho_e) * \varepsilon \tag{3}$$

where ρ_e is the photo-elastic coefficient of the fiber. This parameter will depend on the type of fiber used for the sensor, as it is material dependent. For the remaining work presented, standard telecommunications fiber was used with a core material of fused silica, and therefore the value of $\rho_e \approx 0.22$ was used. At 1550nm, the wavelength shift due to strain is 1.209pm/με. Temperature also has an effect on the Bragg wavelength and does cause a wavelength shift, but we have chosen to exclude this factor in our work. All measurements were performed under uniform temperature conditions.

1.5 Fiber Optic Sensor Manufacturing Process

As previously mentioned, the manufacturing technique for producing these sensors is well known. A UV laser, typically an excimer laser between 193nm to 308nm, is used to cause a change of the refractive index of the core. The beam from the laser is shaped and focused through a photomask that has the desired Bragg grating period, as seen in Figure 7. As the light passes through this mask, only a portion of the UV laser irradiates the fiber and causes the periodic refractive index change. A number of parameters can be tuned in this manufacturing process to vary the reflectivity of the FBG, spectral width and spectral shape.
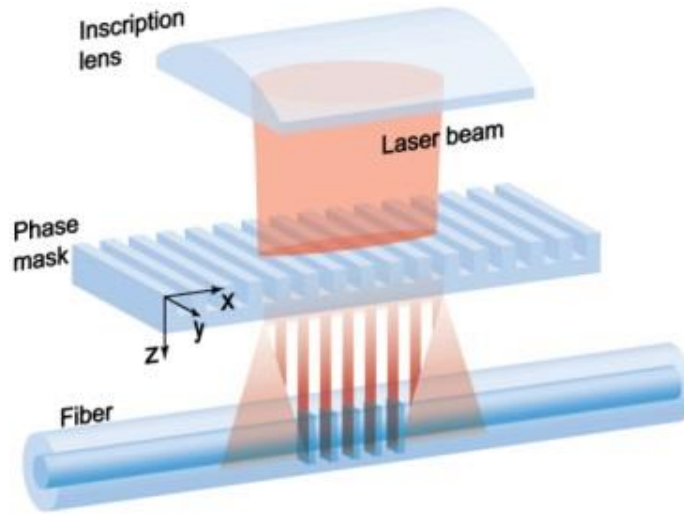
Figure 7 - UV FBG manufacturing process [16].

Other manufacturing techniques do exist for FBG manufacturing. Draw tower gratings, which are FBGs that are formed as the fiber is being manufactured, offer improved mechanical strength but lower reflectivity, as the UV exposure time is limited. Femtosecond lasers are beginning to offer a new, more unique method of FBG inscription as a result of the short pulse duration and high beam energy characteristics of the laser. The work presented utilized the UV laser inscription method for FBG manufacturing, and we will leave it to the reader to further explore alternative manufacturing techniques if desired.

1.6   Fiber Optic Torque Sensors

Prior work has been done towards the design and development of fiber optic torque sensors. Recall that torsion is a measurement of the twist formed in a material due to an applied torque, and therefore we can determine the torque applied by measuring the torsion in a material. Researchers X.G. Tian and X.M. Tao were the first to demonstrate an FBG based torsion sensor that was bonded onto a copper shaft [9]. Utilizing a single-mode silica fiber, the FBG was manufactured using an ArF excimer laser and the wavelength shift was monitored by using an Optical Spectrum Analyzer (OSA). The work presented successfully demonstrated the feasibility of an FBG torsion sensor with a measurement error that was slightly less than 10%.

Pieter Swart from the University of Johannesburg demonstrated a similar torsion sensor with temperature insensitivity [10]. Again, the FBGs were manufactured using the UV inscription technique and had a spectral bandwidth of 0.12nm; both FBGs were monitored using an OSA.

The experiment showed when torque was applied to the shaft and the torsion was measured by the FBG, a wavelength shift of 19.4 pm/N·m and excellent temperature insensitivity was seen. The limitation posed by this research, however, is that of how can we accurately measure the wavelength shifts seen at the sensor.

Optical spectrum analyzers are limited in their ability to resolve below +/-15pm, as is common in most research labs. Commercially available interrogators offer wavelength monitoring accuracy of +/-1pm, such as the Micron Optics si255 interrogator; however the FBGs being used have a large spectral width. With typical FBG spectral widths between 0.1nm to 0.3nm, it is difficult to resolve small wavelength shifts of a few picometres. Measurement requisition rate recently has increased with the latest interrogators, and can now achieve 5000Hz compared to the early limitations of 1000Hz. This, however, will still not be enough for acoustic signals that may be of interest to monitor. In addition to the difficulty of resolving these small wavelength shifts and measurement bandwidth limitations, interrogators that offer this spectral resolution start above $10,000 USD, a cost that often exceeds commercially available electrical torque sensors [11].

1.7   Research Motivation

A comparison of the benefits and limitations of using fiber optic sensors to perform strain measurements vs. that of foil strain gauges is presented in Table 1.

Technology	Benefits	Limitations
Foil Strain Gauges	- Low cost (sensor and measurement device/amplifier) - Well known manufacturing process - Resolution and accuracy can achieve 0.05% FS	- Not intrinsically safe - EMI sensitive
Fiber Optic Sensors	- EMI insensitive - Inherently intrinsically safe - Resolution and accuracy possible can achieve sub 0.01% FS	- Expensive (primarily due to measurement platform) - Bandwidth of measurement systems

Table 1 - Benefits and limitations of strain measurement technology

The unique benefits offered through the use of fiber optic sensors for strain measurement are exciting, as opportunities to perform measurements with better accuracy, in new environments (i.e. high EMI environments) are currently unexplored. The limitations of fiber optic sensors, as presented in Table 1, is that the measurement technology available for fiber optic sensors does

not allow for small wavelength shift monitoring at high speed for a competitive price compared to electrical sensors.

The motivation for this work presents an exciting opportunity to create a high bandwidth (>20kHz) and accurate (sub micro-strain) measurement device that can be used to measure strain in a fiber optic sensor. Developing this device for a cost under $2,000 is also desired, as there is currently nothing commercially available at this price point. Using torsion measurements as a demonstration tool allows us to compare against high end commercially available electrical solutions and against research performed on fiber optic torsion sensors previously.

2. Fiber Optic Sensor Measurement Platform

The system requirements for the measurement platform were determined through the evaluation of the limitations that currently exist with commercial measurement devices. Three primary requirements were to be targets: low cost, high accuracy (small wavelength shift detection) and high measurement bandwidth.

A technical literature review revealed research being done to monitor strain by means of the Pound-Drever-Hall (PDH) laser locking technique; a well-known technique used in telecommunication products to improve lasers wavelength stability over time. Utilizing this technique, a high accuracy platform was developed, along with a matching fiber optic sensor, and it was proven through calibration to be a viable solution for monitoring torsion and achieving resolutions below 0.05% FS torque.

2.1 Pound-Drever-Hall Technique

A common method for improving the frequency stability of a laser, the PDH locking technique matches the laser's center frequency to that of an external, high-finesse Fabry-Perot cavity and locks to a fringe within that cavity [12]. A Fabry-Perot cavity acts as a filter, allowing only frequencies of light that are integer multiples of the cavities free spectral range (FSR) to exist.

$$\Delta v_{FSR} = \frac{c}{2L} \tag{4}$$

where c is the speed of light in a vacuum, and L is the length of the cavity. The transmission spectrum at the output of a Fabry-Perot cavity is presented in Figure 8 with a low finesse to make it easier to see the features. As the spectral width of the transmission peaks decreases with an increase in finesse, the peak of this fringe becomes narrower as well. As the peak of the fringe transmits 100% of the incident light, the intensity of the reflected light will reach 0% at this frequency. This is useful, but limited as the reflected signal is symmetric about resonance at the peak, and if the laser were to shift away from resonance, the reflected signal would not tell you if an increase or decrease in the lasers frequency is needed to bring it back to resonance.
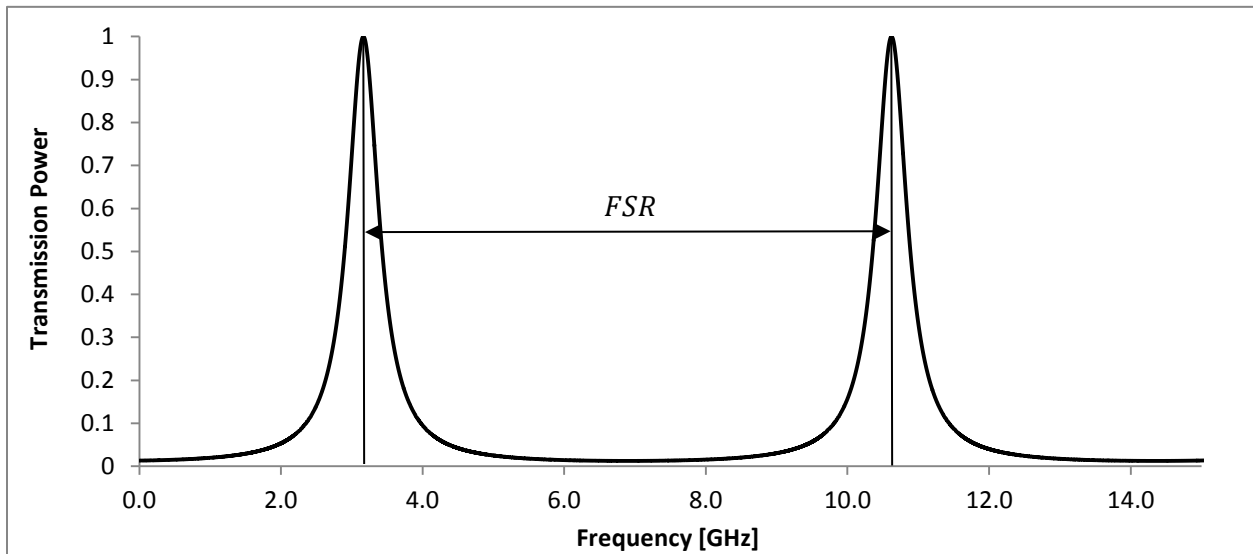
Figure 8 - Transmission spectrum of a Fabry-Perot cavity. This cavity has a finesse of approximately 14 with wide fringes to make illustration easier
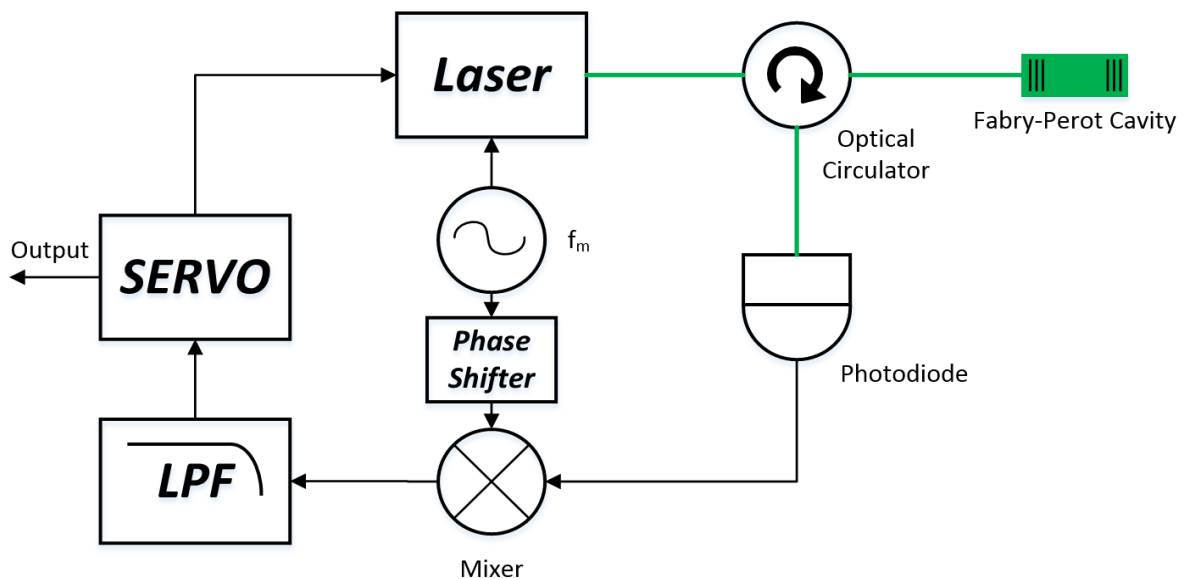
Figure 9 - A current modulated PDH system; optical paths are represented by green lines and electrical paths by black lines.

In order to create an asymmetric signal at the cavities resonance, the PDH technique modulates the lasers frequency and determines the derivative of the reflected intensity. A common PDH setup, where the laser diode is current modulated is presented in Figure 9. In this setup, a local oscillator, f_m, directly modulates the DFB lasers frequency and the reflected signal from the Fabry-Perot cavity is monitored by a high-speed photodiode. The local oscillator and the output

from the photodiode pass through an RF mixer, which is a passive device that outputs the product of the two input signals. The output from the mixer will therefore contain both AC and DC components, of which we are only interested in the DC signal as this is the derivative of the reflected signal. To isolate the DC component, the output of the mixer passes through a low-pass filter, and then into the servo controller which actively monitors the signal and provides an output to the DFB laser to maintain a lock to the cavities resonance.

For an ideal cavity (i.e. no losses), the reflection coefficient is given in equation (5)

$$F(\omega) = \frac{E_{ref}}{E_{in}} = \frac{r(\exp\left(i\frac{\omega}{\Delta\nu_{FSR}}\right) - 1)}{1 - r^2\exp(i\frac{\omega}{\Delta\nu_{FSR}})} \tag{5}$$

where E_{ref} is the electric field of the reflected beam, E_{in} is the electric field of the incident beam, and r is the amplitude reflection coefficient of each mirror. The reflected beam is comprised of two components; the first being the reflected beam off of the first mirror that never entered the cavity, and the second being the leakage beam through the mirror that is exiting the cavity. As the lasers incident beam has a frequency matching that of the cavities resonance, the intensities are equal.

If the laser's frequency is exactly that of the free spectral range of the cavity, the two beams will have the same amplitude, but will be 180° out of phase with each other, as can be seen in Figure 10. If the laser's frequency is slightly off of the free spectral range of the cavity, but not so far off that the reflected intensity is 100%, the phase between the two beams will not be 180°. This difference in phase allows us to determine which side of resonance the laser's frequency is on.
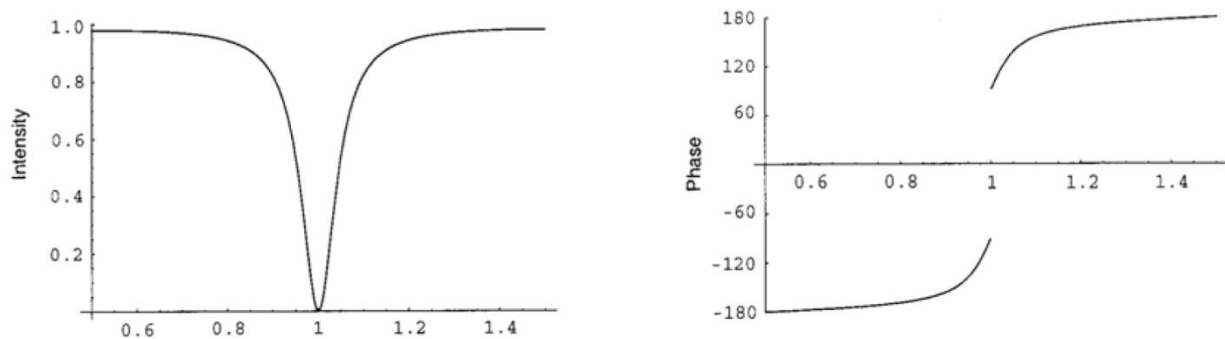
Figure 10 - Reflection coefficient magnitude and phase plots for a Fabry-Perot cavity [12].

As has been described, we need a way to measure the phase of the reflected beam from the Fabry-Perot cavity, which cannot be directly done. Instead, we can modulate the injection current of the laser using a local oscillator to generate sidebands in the electric field of the lasers beam.

$$E_{inc} = E_0 e^{i(\omega t + \beta \sin \Omega t)} \tag{6}$$

where β is the modulation depth and the modulation frequency is Ω. This function can be expanded using Bessel functions to be

$$E_{inc} = E_0 \left[J_0(\beta) e^{i\omega t} + J_1(\beta) e^{i(\omega + \Omega)t} - J_1(\beta) e^{i(\omega - \Omega)t} \right] \tag{7}$$

Through the evaluation of equation (7), the incident field is comprised of the carrier frequency at ω and two side sidebands at ω Ω. The reflected beam's power from the cavity is measured by the high-speed photodiode and is shown in equation

$$P_{ref} = |E_{ref}|^2 = |E_{inc} F(\omega)|^2 \tag{8}$$

$$
\begin{aligned}
P_{ref} = \; & P_c |F(\omega)|^2 + P_s |F(\omega - \Omega)|^2 \\
& + 2\sqrt{P_c P_s} \{ Re\big(F(\omega) F^*(\omega + \Omega) - F^*(\omega) F(\omega - \Omega) \big) \cos \Omega t \\
& + Im(F(\omega) F^*(\omega + \Omega) - F^*(\omega) F(\omega - \Omega)) \sin \Omega t \} \\
& + (2\Omega \; terms)
\end{aligned}
\tag{9}
$$

where the power of the carrier and power of the sidebands are reflected as P_c and P_s, respectively. The component of the equation that contains the information about the lasers frequency, and therefore is the component that we are interested in measuring, is $F(\omega)F^*(\omega + \Omega) - F^*(\omega)F(\omega - \Omega)$.

This component can be extracted by multiplying the detected signal, P_{ref}, with the initial modulation frequency that was provided to the laser through the local oscillator. This multiplication is performed by the mixer, which generates an output that contains one time independent term and multiple time dependent terms. The time dependent terms are then removed by the low-pass filter.

One needs to ensure the phase of the signal from local oscillator is correct so that the product of the two signals will generate a time independent term from the mixer. Recall that the product of two sine waves is

$$\sin \Omega t \sin \Omega t = \frac{1}{2} - \frac{1}{2} \cos 2\Omega t \qquad (10)$$

which, after we pass through the low-pass filter will generate the desired time independent error signal presented in equation (11).

$$error\ signal \approx \sqrt{P_c P_s}\big(F(\omega)F^*(\omega + \Omega) - F^*(\omega)F(\omega - \Omega)\big) \qquad (11)$$

An error signal, as mathematically described above, was measured from the platform developed and is shown in Figure 11. The slope of the error signal determines the sensitivity of the PDH system, and to measure small wavelength shifts accurately, it is desirable to have this slope be as high as possible. This can be done by optimizing a few parameters; the first is the reflectivity of the mirrors that make up the Fabry-Perot cavity. The higher the reflectivity, the narrower the spectral width of the cavity fringe will be. The second is to increase the distance between the mirrors, as the spectral width of the cavity fringe will decrease as the cavity length increases. The third method is to optimize the ratio between the powers of the carrier frequency and the sidebands, with an optimum ratio between the carrier and one sideband being ½.
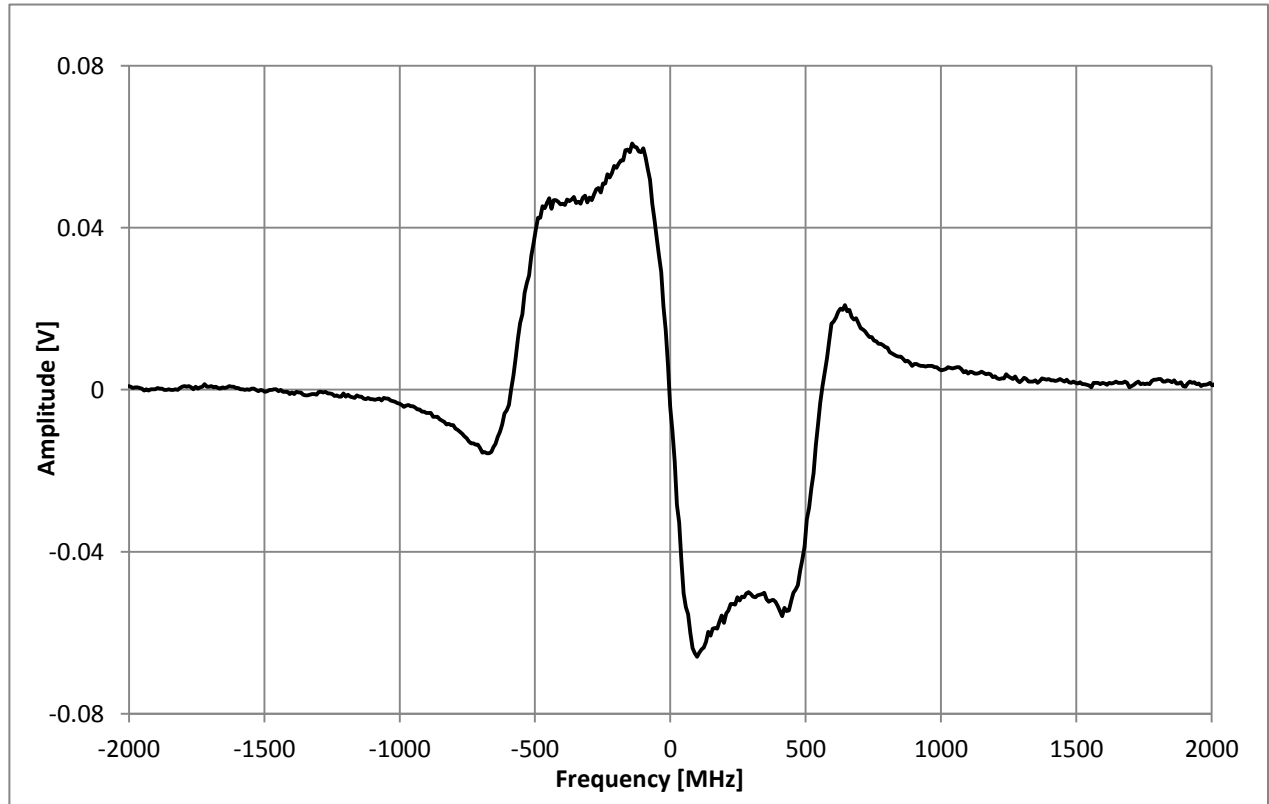
Figure 11 - PDH error signal; modulation frequency approximately 130MHz

2.2 Fiber Bragg Grating Fabry-Perot Sensor

The quality of the Fabry-Perot cavity, as presented in the previous section, is critical in improving the sensitivity of the system. In order to improve the sensitivity to small changes, and in order for us to monitor those small wavelength shifts, we need to produce a Fabry-Perot cavity that has narrow fringes that the PDH platform can lock to. As we want to monitor strain in a material, similar to how a foil strain gauge works, we need to create this Fabry-Perot cavity within a small, low mass component such as optical fiber.

A Fabry-Perot cavity is formed by utilizing two mirrors that only allow particular frequencies of light to propagate. By manufacturing two FBG's at the same Bragg wavelength within an optical fiber, spaced apart at a known distance, we can create an in-fiber Fabry-Perot cavity. The design of this sensor is presented in Figure 12. There are three critical parameters that will define the characteristics of the sensor: The center-to-center distance between the two FBGs, the length of the FBGs, and the reflectivity of the FBGs.

It is desirable, as seen by the sizes of commercially available foil strain gauges, that the sensor be as small as possible. For the work presented, Corning SMF-28 fiber was used which has an uncoated cladding diameter of 125μm and a core diameter of 8.4μm. To improve bonding strength to other materials, after manufacturing the FBGs, the fiber was recoated with polyimide.
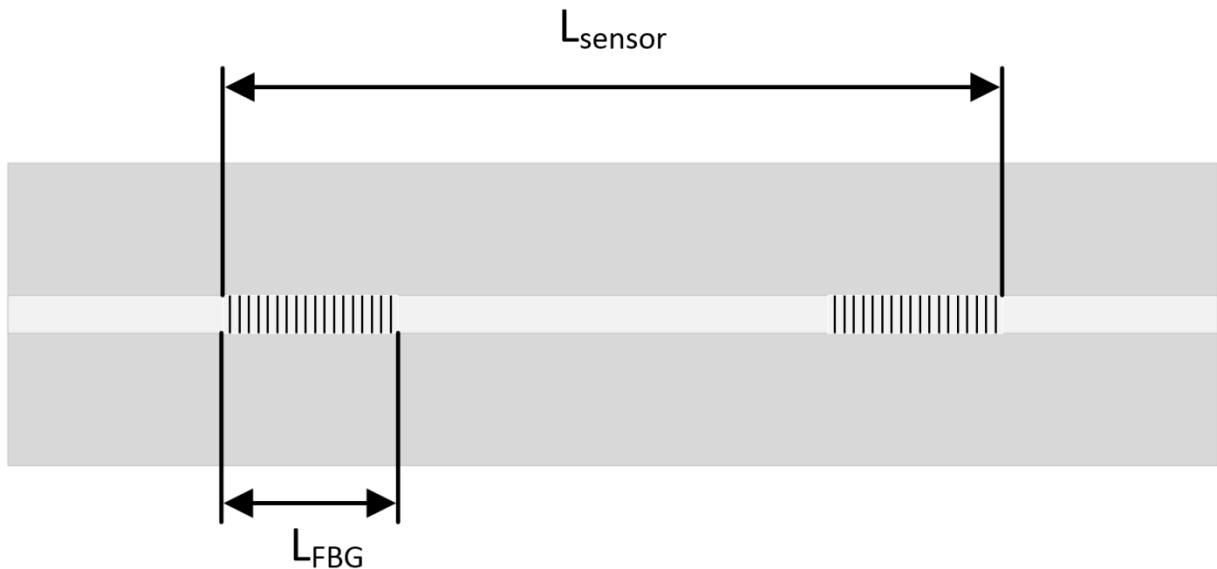
Figure 12 - FBG Fabry-Perot cavity within the core of the fiber. Two critical parameters are the length of the FBG and overall sensor length.

After recoating, the diameter of the fiber is approximately 140µm. The length for each FBG made in Ryerson's lab is 5mm. The overall length of the sensor is a parameter that can then be tuned, but it will affect the spectral width of a cavity fringe and the free spectral range. This is illustrated in Figure 13 and summarized in Table 2; as the cavity length increases, both the free spectral range and the spectral width of the fringes decrease while R is kept the same.

Sensor Length [mm]	Free Spectral Range [pm]	Spectral Width [pm]
10	114.49	1.49
20	47.68	0.62
50	17.34	0.23

Table 2 - Effects of changing the sensor length on Fabry-Perot cavity parameters with fixed FBG reflectivity
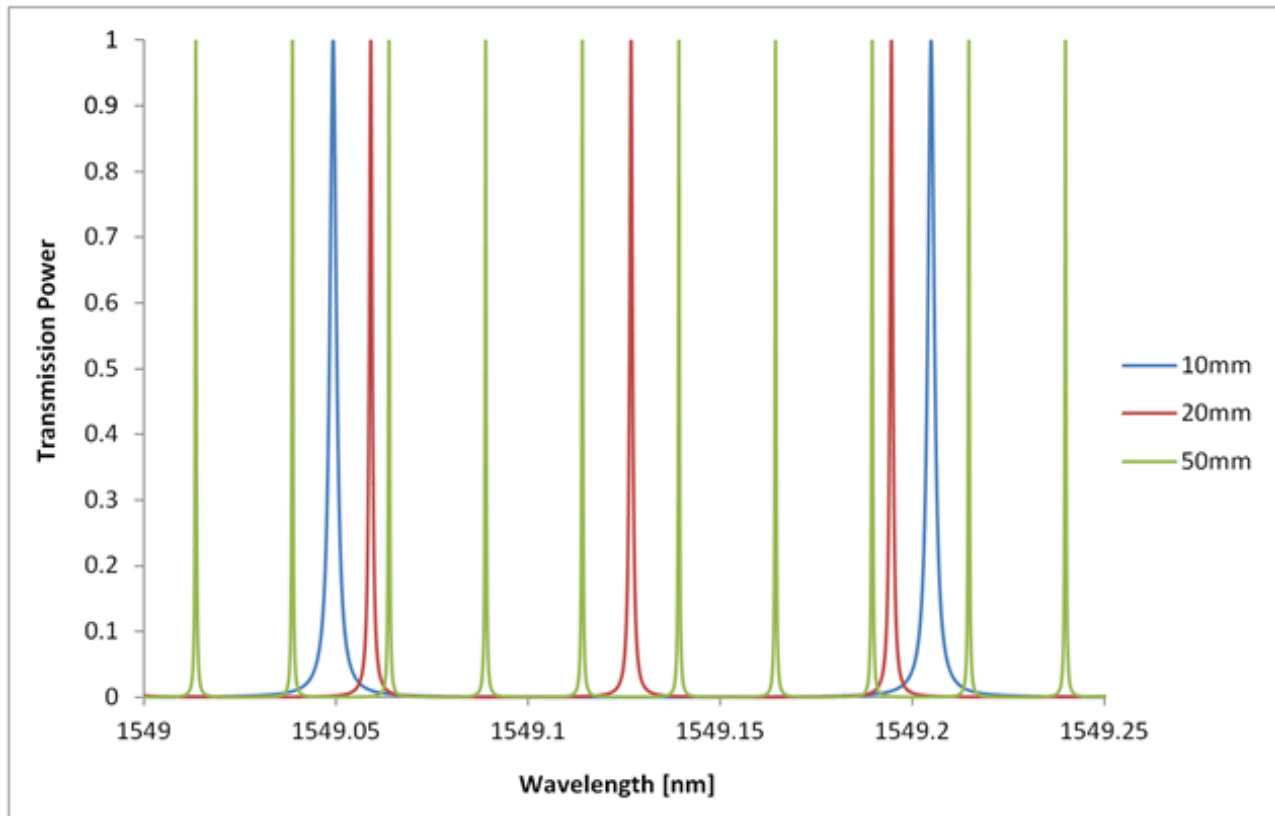
Figure 13 - Transmission spectrum of Fabry-Perot cavity with varying cavity lengths.

The reflectivty of the FBG is the third component that can be adjusted, and will have a direct impact on the spectral width of the fringes. With the UV manufacturing technqiue for the FBG's, we have the ability to control the reflectivity of the FBG's quite well. A summary of the effect of varying the FBG's reflectivty is presented in Table 3.

Reflectivity [%]	Free Spectral Range [pm]	Spectral Width [pm]
50	42.98	9.67
80	45.15	3.21
90	46.41	1.56
99	49.04	0.16

Table 3 - Effect of varying the reflectivity of the FBG's with a fixed FBG length and cavity length.

It can be seen that in order to achieve the narrowest spectral width of a cavity fringe we need to manufacturer the FBG's with a large cavity length and a high reflectivity. The cavity length needs to be considered carefully, as we wish to apply a uniform strain to the fiber, and doing this can be difficult if the sensor is long. In addition, it can be difficult to package a sensor that is longer than 30mm, as this is the typical size for a strain gauge used for torsion measurements.

Achieving a high reflectivity can also pose a problem during FBG manufacturing due to a phenomenon known as birefringence. Although we are using a single-mode fiber, two modes, orthogonally polarized, exist. If the fiber is perfectly circularly symmetric, the two modes would propagate through the fiber at the same velocity. Due to imperfections in the fiber, however, these two modes propagate with small differences in their phase. During the manufacturing of high reflectivity fibers, the possibility of experiencing birefringence increases. A lot of research has been done to characterize and understand birefringence in FBG manufacturing, and a great resource for further details can be found in the work presented by Rachid Gafsi, *et al* [13].
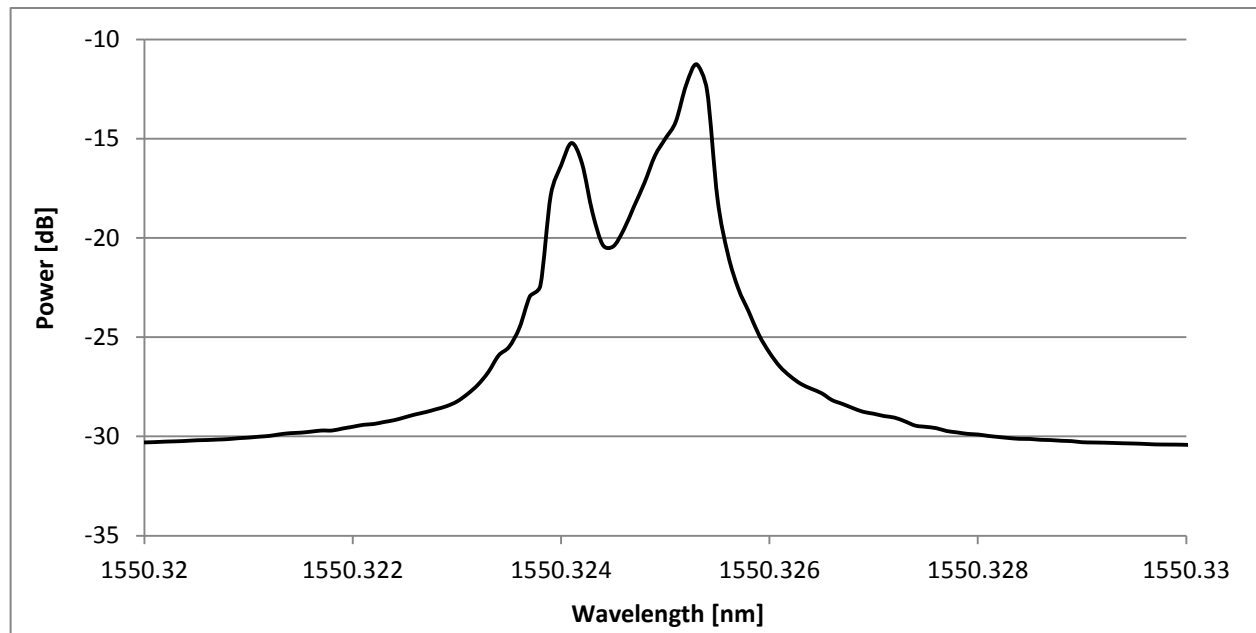
Figure 14 - Birefringence (split peak) seen in Fabry-Perot cavity fringe.

18
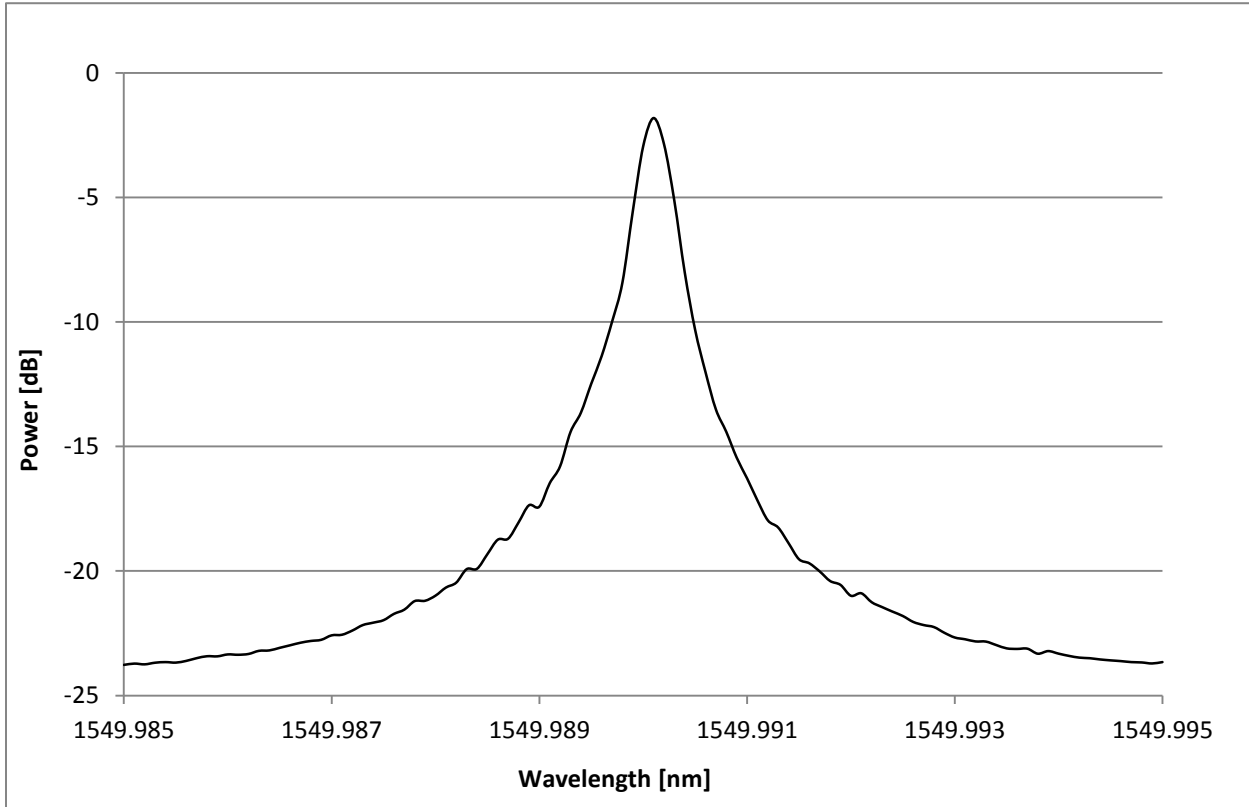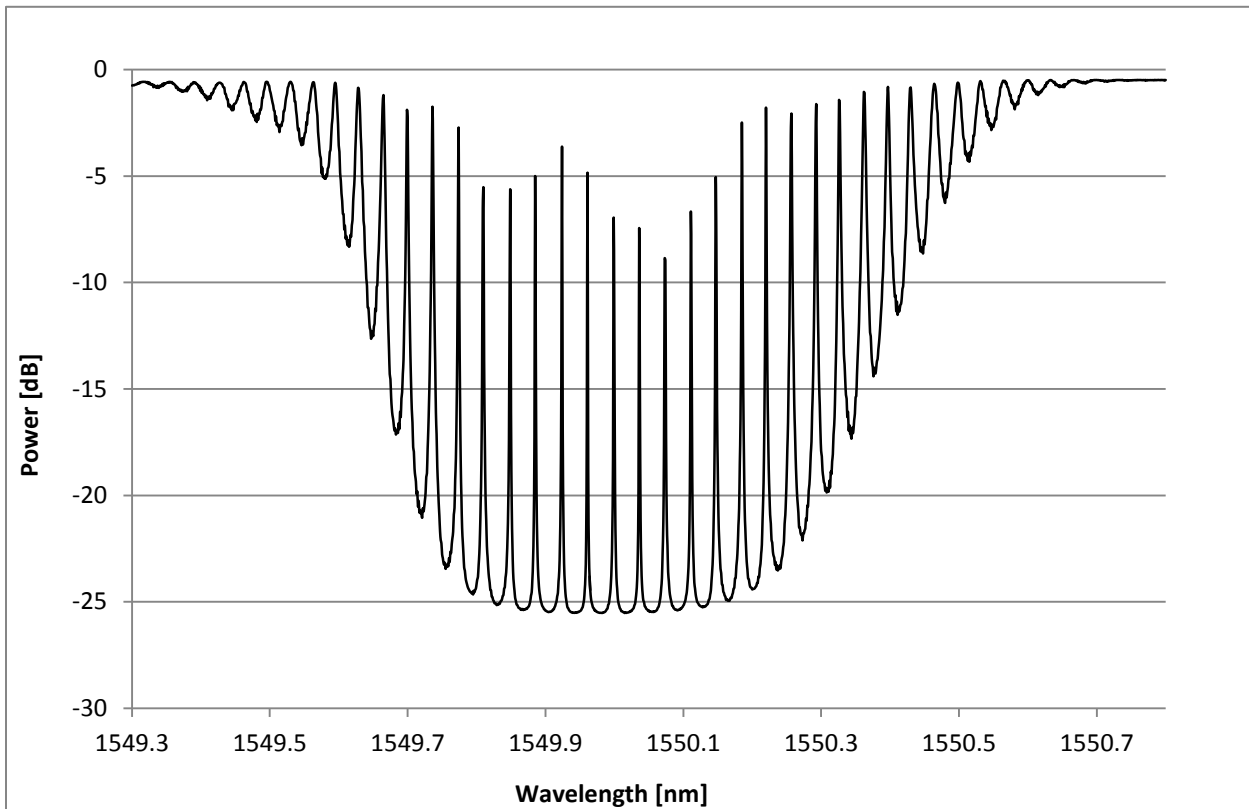
Figure 15 - Top: FBG Fabry-Perot transmission spectrum Bottom: Middle cavity fringe peak at 1549.990nm

Birefringence can be seen in the transmission spectrum of a sensor as the splitting of the Fabry-Perot cavity fringe, as seen in Figure 14. As the PDH system will be attempting to lock the lasers frequency to that of the peak of a cavity fringe, birefringence would cause instability and potentially prevent the lock from successfully working.

Based on experimentation through manufacturing, and picking a length that is similar to that of existing foil strain gauges, the fiber optic sensor design settled on the following parameters: L_{FBG} = 5mm, L_{sensor} = 27mm, R ≈ 99%. Each FBG is apodized with a SINC function. The sensor was manufactured in Corning SMF-28 fiber and recoated with polyimide. The sensors transmission spectrum and middle cavity fringe can be seen in Figure 15. The spectral width of the peak is 0.5pm with no birefringence and a free spectral range of approximately 38pm.

2.3 PDH Measurement Platform

A key motivation behind this research was to develop a high accuracy, low cost strain measurement platform that could highlight the benefits of optical sensors and compete directly against electrical solutions like the foil strain gauge. Typical amplifier costs for a foil strain gauge range between $1,000 - $2,500, depending on the accuracy requirements and manufacturer. To demonstrate the viability of a low cost measurement platform, the target price was set to $2,000 in low volume pricing.

In addition to the cost, the accuracy and the measurement bandwidth requirements were unique, so it was determined that a custom PDH platform would be developed similar to that presented in Figure 9. Utilizing an external modulation device, such as an electro-optic modulator (EOM), to generate the sidebands on the output of the laser was considered, but the cost for these external devices is over $1,000 and too expensive for the intended device.

As the platform has many different components, development was broken down into multiple tasks with the primary focus being on control of the DFB lasers wavelength. As the measurement accuracy depends on the ability to lock the lasers frequency to that of a fringe within the FBG-FP sensor, it was critical to focus on the control of the lasers current and temperature. The first prototype developed only had a custom current and temperature controller for the DFB, and used off the shelf components for the other items. After successful proof of operation, the second prototype was designed and built that relied less on off the shelf components, with only the

photodiode receiver being a purchased item. Future work will include the design and development of a custom photodiode receiver.

2.3.1 PDH Measurement Platform – Prototype 1

The DFB laser used for the first prototype was a Lucent D2526G35 with a quoted line width between 2-10MHz that had an internal bias-T network for RF modulation. The operating range of the diode is between 15°C and 35°C, with the temperature controlled by an internal Thermal Electric Cooler (TEC). The threshold current for the diode is between 20-30mA, with a maximum operating range of 100mA for 6.0mW of output power.

In order to maintain the lock of the laser to the external FBG-FP sensor, based on the error signal feedback, the platform either adjusts the current to the diode or the temperature of the diode, depending on the magnitude and rate of the change in strain seen at the sensor. For large changes in strain, the temperature of the diode is adjusted as the tuning parameter is large; 0.95nm/°C. It can be seen through this parameter that it is difficult to accurately control the output wavelength of the laser based on temperature, as adjusting the temperature of the diode with an accuracy of 0.01°C would only adjust the output of the laser by 0.95pm. The rate of change of the temperature of the diode is also limited, and was measured to be approximately 200ms for every 1°C of temperature change.

To accurately maintain the lasers output wavelength, current control is used. It was determined through experimentation, that the DFB's change in wavelength due to a change in operating current is 4pm/mA. This value is not specified by the manufacturer, but can clearly be determined from the slope of the lasers operation current vs. output wavelength presented in Figure 16. It can be seen that this value does not deviate based on the diodes operating temperature.

The current control of the diode is therefore critical towards achieving the accuracy and the measurement bandwidth for the sensor. It was decided to allow for two methods of current control of the laser diode; the first being DC current control and the second being a high-speed current control of +/-9mA. The DC current control is used to select the nominal operating current of the diode between 0mA and the maximum operating current of 100mA. This current is set by varying the voltage of a 16-bit, 0-5V digital-to-analog converter (DAC) across an accurate, fixed
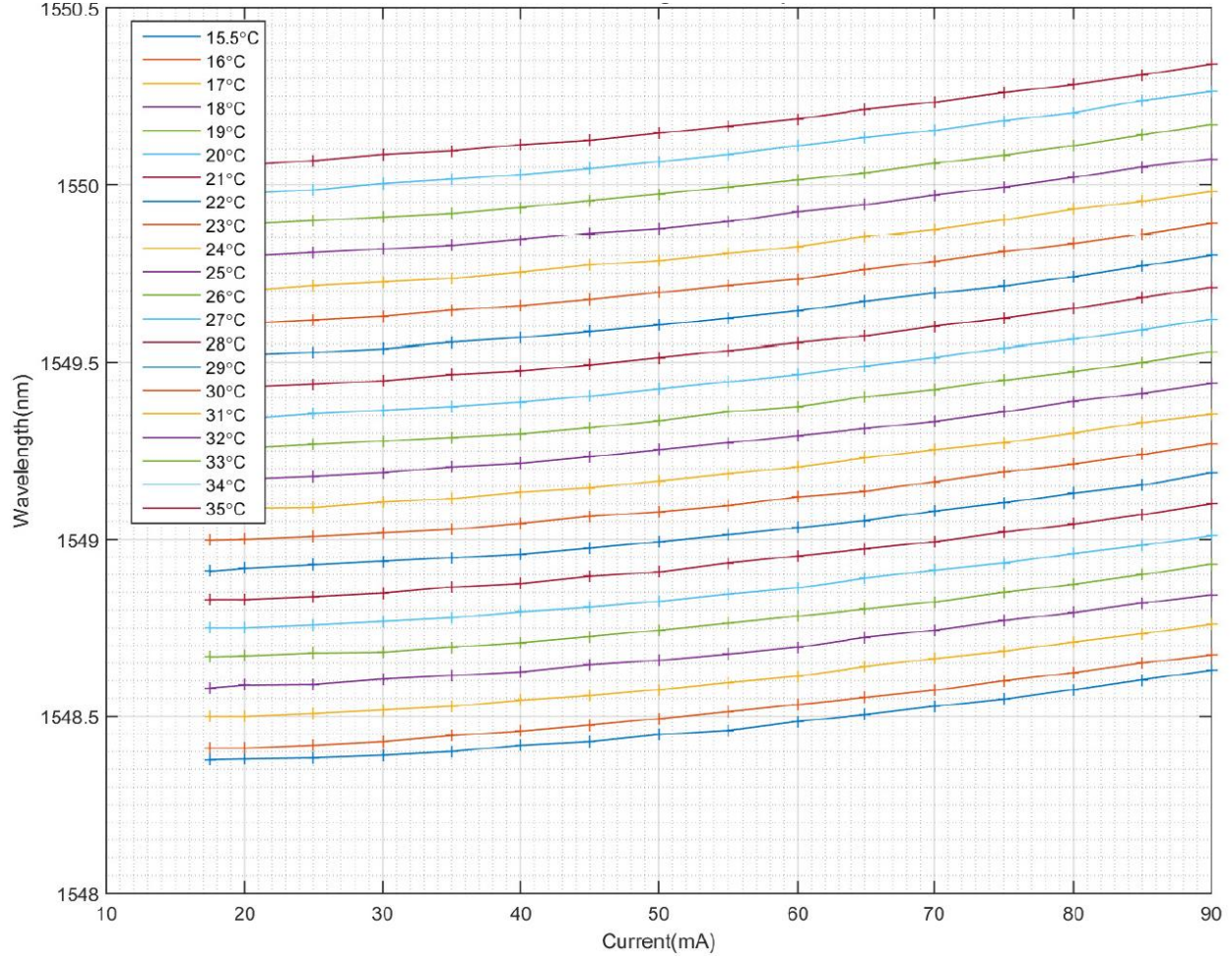
Figure 16 - D2526 DFB laser - operating current vs. output wavelength at different TEC temperatures.

resistor and a known regulated voltage. The value of the current can be determined using equation (12).

$$I = \frac{V_{REG} - V_{DAC}}{R} \tag{12}$$

The set point accuracy of this DC current, while using a 50Ω resistor, is approximately +/- 0.0015mA, which achieves a wavelength shift accuracy of +/-0.006pm. Through this control, we can accurately set the nominal current value of the diode.

In order to respond to high-speed, low amplitude changes in strain (i.e. acoustic measurements between 20Hz – 20kHz), a second stage of current control was added. This current can be modulated through another 16-bit DAC as fast as 1MHz from -9mA to +9mA off the nominal set

diode current. The accuracy this DAC can achieve in current control is +/-0.2µA, which achieves a wavelength shift accuracy of +/-0.001pm.

The first prototype circuit can be seen in Figure 17, where the custom circuit is the purple Printed Circuit Board (PCB) at the bottom of the image. The RF components required for use in the PDH system were purchased from Mini-Circuits. To reduce complexity and ease development, an off-the-shelf Arduino controller was used to control the DAC's and TEC controller within the circuit. A National Instruments data acquisition card, PCIe-6351, was used to record the error signal from the photodiode receiver and operate a LabVIEW PID control loop to maintain the lasers lock to the FBG-FP sensor.

The platform was a successful demonstration of the current and TEC controller for the laser diode; however the cost was still too high due to the other hardware. In addition, the PID control loop operating through LabVIEW was limited to only 500Hz; well off the desired rate of 40kHz.
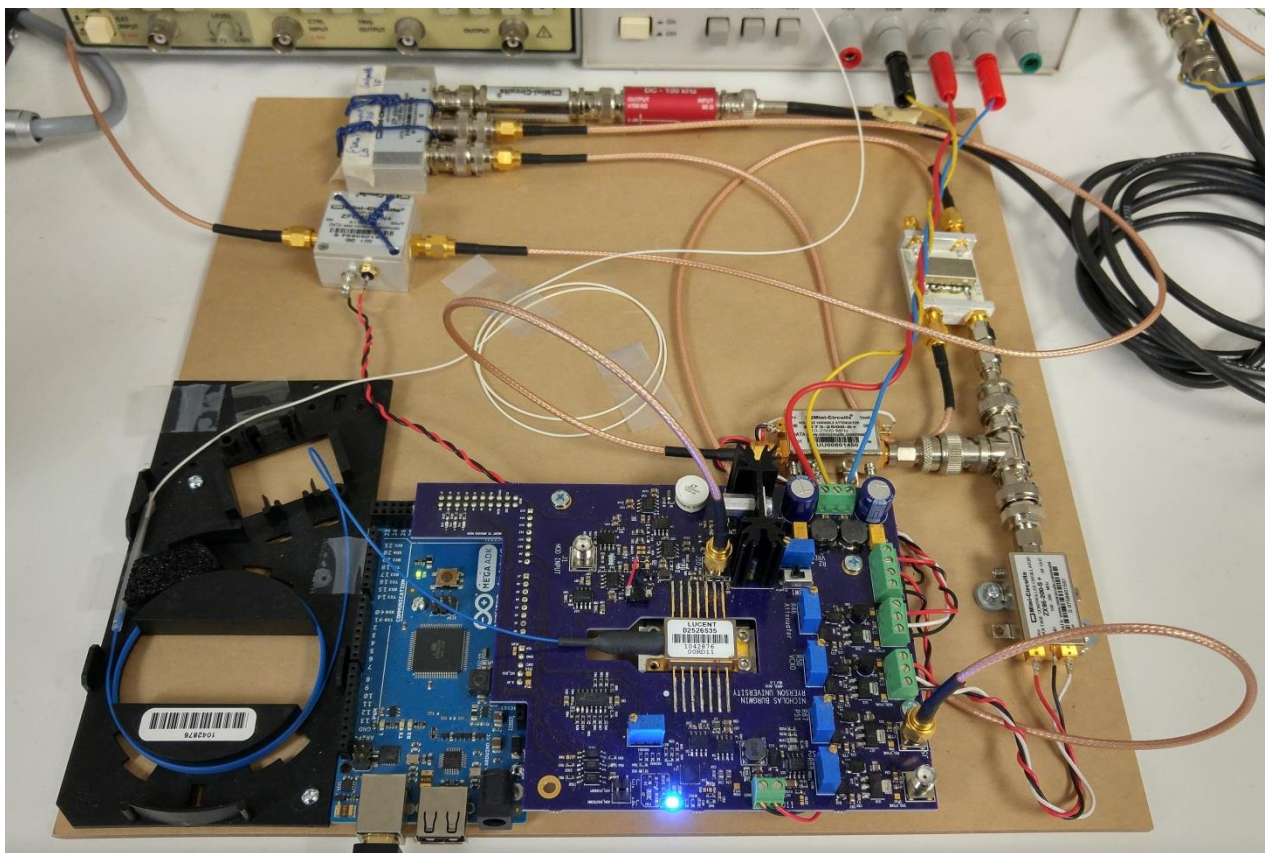
Figure 17 - PDH Measurement Platform - Prototype 1. The purple PCB at the bottom of the image is the custom laser diode controller.

2.3.2 PDH Measurement Platform – Prototype 2

To improve the PID control loop speed, and therefore increase the measurement bandwidth the platform can achieve, an embedded controller was selected for the second prototype. As we were eliminating the need for LabVIEW, we needed to include an analog-to-digital converter (ADC) to monitor the error signal, and a DAC to provide an analog output that is proportional to the strain experienced by the fiber.

With a solid understanding of the operating characteristics of the laser, an evaluation of the analog output accuracy was done before completing the design and selecting all the components. The system requirements and parameters used to determine the systems accuracy is presented in Table 4.

Strain Measurement Parameters	Value	Unit	Notes
Laser Diode Temperature Range	20	°C	
Wavelength Shift per °C	95	pm	
Wavelength Shift due to Temp.	1900	pm	
D2526 Current Tuning	4	pm/mA	Measured
Delta Operating Current Range	60	mA	(30mA to 90mA)
Wavelength shift due to current	**240**	**pm**	
Combined Total Wavelength Shift	2140	pm	Temperature + Current
Practical Range	90	%	
Wavelength Tuning Range	**1926**	**pm**	
Strain vs. Wavelength Shift	1.209	pm/με	
Maximum Strain Measureable	2328.5	με	
+/- Strain	**1164.3**	**με**	

Analog Output Requirements	Value	Unit	Notes
Analog Output Range (0 - 5V)	2328.5	με	0V = 0με, 5V = 2328.5με
Desired Accuracy of Gauge (+/-)	0.01%		
Strain Accuracy (+/-)	0.233	με	
Number of Discrete Steps	10000	steps	
Minimum Voltage Output Step	0.5	mV	
Minimum Analog Output ADC bits	**13.29**	**bits**	

Table 4 - Analog output accuracy requirement check for Prototype 2

Based on the tuning range of the lasers temperature and current, and when measuring the strain in a FBG with a Bragg wavelength near 1550nm, the maximum strain measurement that can be

monitored is approximately 2300με, limited by the lasers tuning range. It is worth noting that prior research has been performed by Paulo Antunes, *et. al*, regarding the mechanical properties of single-mode optical fiber [14]. The group performed tensile tests on both coated and non-coated SMF-28 fiber, and noted the average tensile force that caused the fiber to break. Using the maximum tensile strength values that were measured, the relative elongation, and therefore the axial strain experienced by the fiber can be determined. The results are presented in Table 5.

Maximum Tensile Strength			
Parameter	Value	Unit	Notes
Average w/ acrylate coating	24.6	N	+/-2.38N
Tensile Strain	0.029	ε	
	28959.7	με	
Relative Elongation	2.90%		

Average w/o coating	4.35	N	+/-1.45N
Tensile Strain	0.005	ε	
	5120.9	με	
Relative Elongation	0.51%		

Table 5 - Maximum axial strain before failure of SMF-28 optical fiber

Data is presented for both a fiber that is coated in acrylate and without any coating at all; that is to say it is just the bare glass of the cladding and core material. There is a large difference between the two measured results, but in both cases, the maximum strain that the PDH platform can measure is below the damage threshold of the fiber. For completeness, a tensile test would need to be performed with a fiber coated in polyimide to confirm the maximum strain tolerable.

The second prototype utilized a 16-bit DAC for the analog output, generating a 0-5V signal that is proportional to the strain experienced by the fiber. The Raspberry Pi 3 was selected as the embedded controller because of the capabilities of the Broadcom processor and ability to improve the operational speed of the PID control loop. Utilizing this controller, vibrational strain has been successfully recorded up to 5kHz and is capable of measuring up to 40kHz. The prototype is presented in Figure 18, and it is quickly seen that the electronics have been split into separate boards. This was done to reduce complexity and risk in case there was an error in a particular circuit. The design has been split into 3 main boards: the laser diode control board, the RF board, and the photodiode receiver. An off-the-shelf photodiode receiver is currently being used, but will soon be replaced by a custom solution.

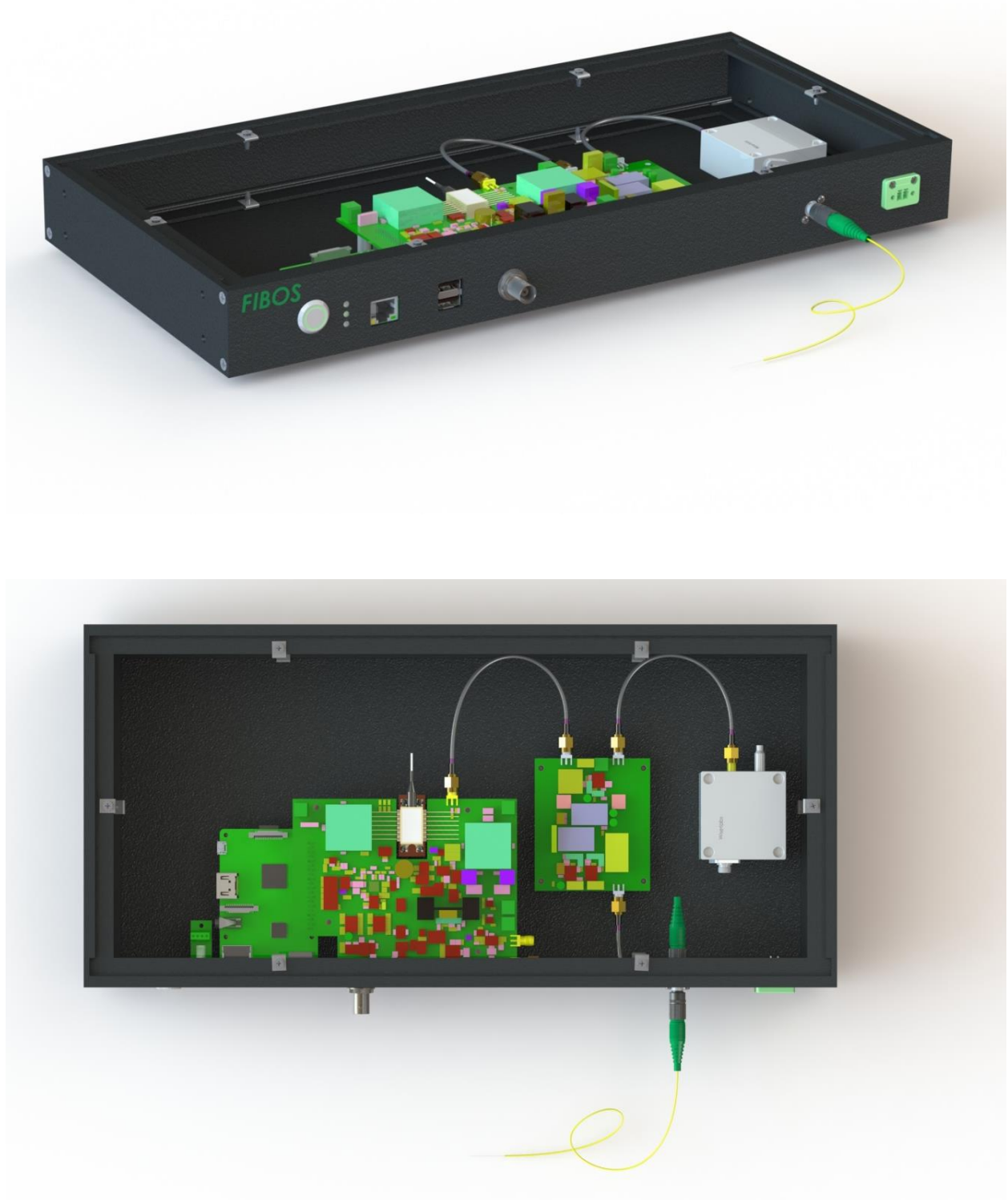**Figure 18 - PDH Prototype 2. The Raspberry Pi 3 is located on the left, with the laser diode control board mounted on top of the Raspberry Pi 3. The RF components are located to the right of the control board, with impedance matched traces to ensure signal integrity on a dedicated PCB. An off-the-shelf high-speed photodiode receiver is to the right of the RF board, which will soon be replaced by a custom photodiode receiver.**

2.4   PDH Measurement Platform Strain Calibration

Before conducting any torsion measurements with the unit, a comparison was done to ensure the wavelength shift measured by the PDH platform was appropriate. To compare against the PDH platform, an Agilent 8164A tunable laser was used as it is a device that can achieve a measurement accuracy of 0.1pm. To create a known wavelength shift, a mass was hung from the fiber to apply a known strain which would cause a known wavelength shift. The material properties of the SMF-28 single-mode cable were used to determine the expected wavelength shift of the FBG due to a hanging mass of 13.78pm/gram. The expected wavelength shift for a number of weights is presented in Table 6.

Mass Added (mg)	Expected Strain (με)	Expected Wavelength Shift (pm)
200	2.31	2.76
500	5.77	6.89
1000	11.55	13.78
1500	17.32	20.67
2000	23.10	27.56
2200	25.41	30.32
2500	28.87	34.46
3000	34.65	41.35
3500	40.42	48.24
3700	42.73	50.99

Table 6 - Hung weight vs. expected wavelength shift in FBG-FP sensor

As both the measurement devices require interrogation of the FBG-FP sensor to be done by the internal laser within each unit, the test was conducted back to back. The fiber with FBG-FP sensor was suspended vertically and a known mass was added to the end of the fiber. A measurement was taken when the fiber and mass settled to a stationary position. As shown in Figure 19, the performance of the PDH platform vs. the Agilent was excellent, with an R-squared value of 0.9997. Further testing needs to be conducted to evaluate the performance of the PDH system over large strain application, however, the data presented here was a successful demonstration of the units ability to accurately measure a wavelength shift experienced by the sensor.
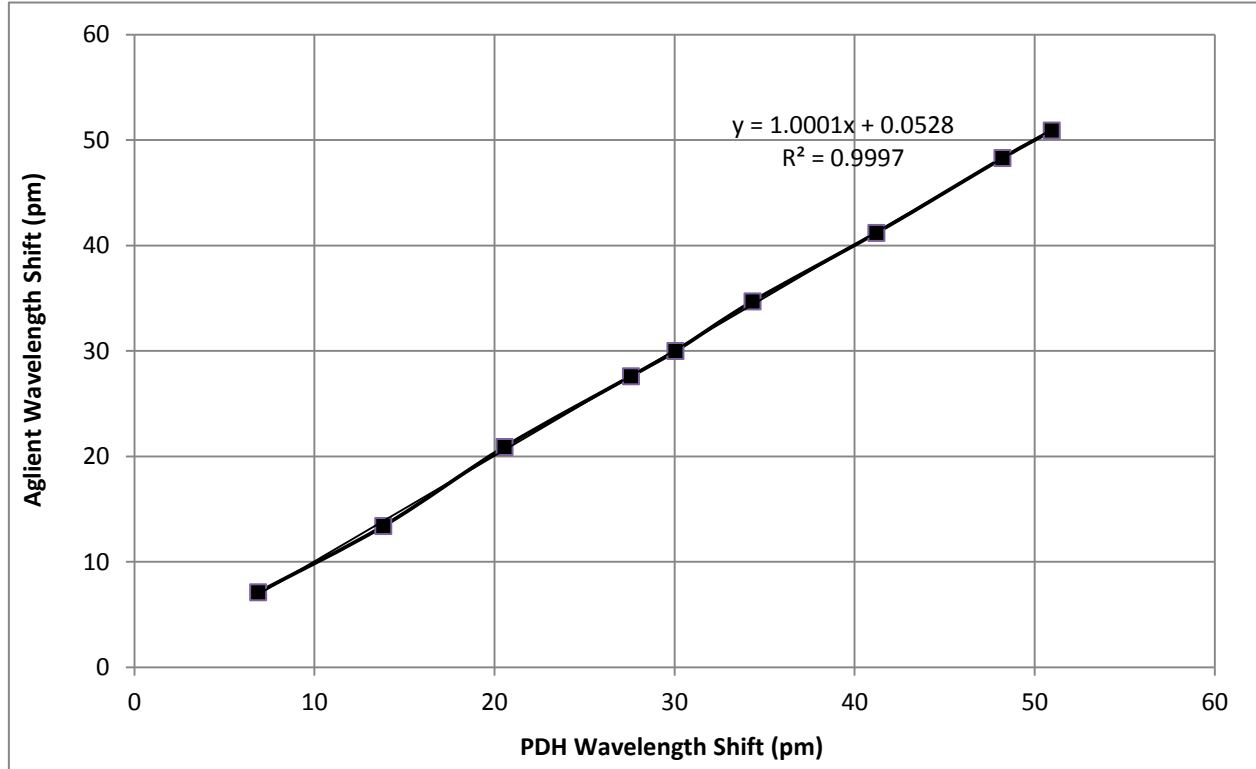
Figure 19 - PDH wavelength shift vs. Agilent wavelength shift due to known strain applied to FBG-FP sensor.

2.5 FBG-FP Torsion Measurements

Strain is defined as the ratio of the change in length of a material from the nominal length. In order to determine the wavelength shift experienced by the sensor, we must first determine the mechanical strain that is applied to the sensor through the application of torque on the shaft. For a solid shaft with a uniform circular cross section, which was what was used in the experiments conducted, the angular defection, θ, of the shaft can be determined by

$$\theta = \frac{T * L}{J * G} \tag{13}$$

where T is the applied torque, L is the length of the shaft, J is the second polar moment of area of the shaft's cross section (shear modulus), and G is the modulus of rigidity. The wrap angle of the sensor on the shaft, α, is critical to define as it will determine the amount of strain experienced by the sensor. As the largest strain is experienced at an angle of 45° off the horizontal axis, a well-known angle when using foil strain gauges for torsion measurements, the fiber is wrapped around the shaft at 45° as well, as seen in Figure 20.

28
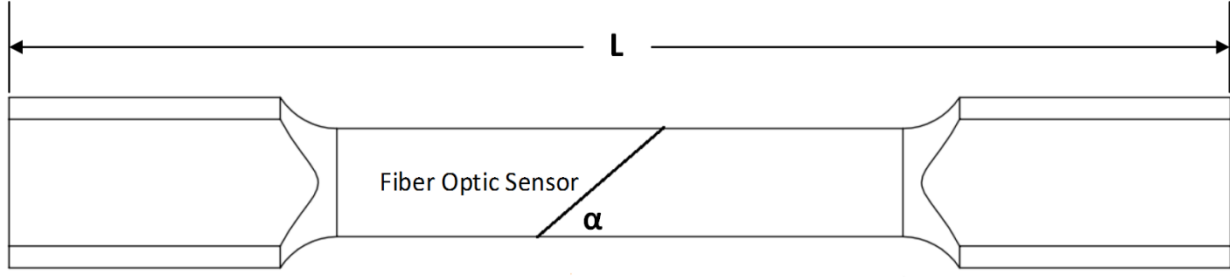
Figure 20 - Aluminum 6061-T6 test specimen with a fiber optic sensor bonded at a wrap angle of α = 45°.

The nominal length of the sensor is $L_s = L / \sin\alpha$, where L is the length of the shaft. As the sensor is bonded to the shaft, and if we assume a perfect bond between the sensor and the shaft, the change in length of the fiber will match that of the shaft. The length of the fiber after an applied torque would be [9]

$$L_s' = \sqrt{L^2 + [\frac{L}{\tan\alpha} + (R+r) * \theta]^2} \tag{14}$$

where R is the radius of the shaft, and r is the radius of the fiber optic sensor. The strain applied to the fiber optic sensor through the application of torque would then be

$$\varepsilon_s = \frac{L_s' - L_s}{L_s} = \frac{L_s'}{L_s} - 1 \tag{15}$$

$$\varepsilon_s = \sqrt{L^2 + \left[\frac{L}{\tan\alpha} + (R+r) * \theta\right]^2} * \frac{\sin\alpha}{L} - 1 \tag{16}$$

simplifying the equation through trigonometric substitutions, we can determine the strain in the fiber to be

$$\varepsilon_s = \sqrt{1 + \sin2\alpha * (R+r) * \frac{\theta}{L} + \left[\sin\alpha * (R+r) * \frac{\theta}{L}\right]^2} \tag{17}$$

Equation (17), if the angle of twist over the shafts length is small, can be simplified to solve for the strain applied to the fiber as a result of the applied torque, T, as presented in equation (19).

$$\varepsilon_s = \frac{\theta * (R+r) * \sin2\alpha}{2 * L} \tag{18}$$

$$\varepsilon_s = \left(\frac{T * L}{J * G}\right) * \frac{(R+r) * \sin2\alpha}{2 * L} \tag{19}$$

Recall that strain applied to the fiber optic sensor causes a wavelength shift away from the nominal Bragg wavelength of the sensor, and as seen in equation (3). Adjusting the terms of this equation to represent the strain experienced by the fiber is shown in equation (20).

$$\varepsilon_s = \frac{\Delta\lambda}{(g * \lambda_o)}$$ (20)

where g is the gauge factor, 0.78, of the fiber optic sensor and is dependent on the fiber material, which is SMF-28 this application. If we substitute equation (20) into equation (19), we can determine the wavelength shift as a result of the torsion caused by the applied torque on the shaft, as shown in equation (21).

$$\Delta\lambda = \left(\frac{T * L}{J * G}\right) * \frac{(g * \lambda_o) * (R + r) * \sin 2\alpha}{2 * L}$$ (21)

3. Torque Experiment Setup

To evaluate the performance of the PDH system through the measurement of torque, a method of applying a known torque was needed. Although a static fixture could have been created, to better evaluate the dynamic performance capabilities of the PDH platform, a torsion test machine was used that is capable of applying dynamic torque to a test specimen, as well as holding a static torque. An aluminum specimen was manufactured according to industry standards and before measuring the torque by the PDH system, the Agilent 8164A tunable laser was used to calibrate and confirm the wavelength shift seen by the FBG-FP sensor.

3.1   Experiment Equipment

The torsion test machine used throughout the experiments was a SANS CTT202 Torsion Testing Machine, which is designed to follow the international standard outlined in ASTM-E143-13, *"Standard Test Method for Shear Modulus at Room Temperature"* [15]. The machine claims a torque measurement accuracy of +/-1% of the indicated torque, based on an internal torque sensor. The data, after the test is performed, is provided as filtered data with a measurement frequency of approximately 16 Samples per Second (SPS).

The torsion rod manufactured for the experiment followed the design guideline provided by the ASTM-E143-13 standard [15]. The shape looked like the rod that was presented in Figure 20, with an overall length, L = 225mm and a diameter of 19.98mm in the middle where the sensor was bonded. The material of the rod selected was Aluminum 6061-T6 as it is an aircraft grade material with well-known material properties. The drawing of the rod is presented in Appendix A, and the test setup with the rod installed in the machine is presented in Figure 21.

The output from the PDH Prototype 2 platform was logged using the National Instruments PCIe-6351 analog card. In addition to recording the strain of the shaft through the fiber optic sensor, four strain gauges were bonded to the rod to measure torsion in a Wheatstone bridge configuration with a Texense XN4-V2 strain gauge amplifier. An image of the torsion rod with the FBG-FP sensor and foil strain gauges bonded is shown in Figure 22. Both the FBG-FP sensor and the foil strain gauges were bonded to the rod using a low viscosity cyanoacrylate.

Figure 21 - Torque Experiment Setup. The aluminum torsion rod with both the fiber optic sensor and foil strain gauges is mounted in the SANS CTT202 Torsion Test machine.
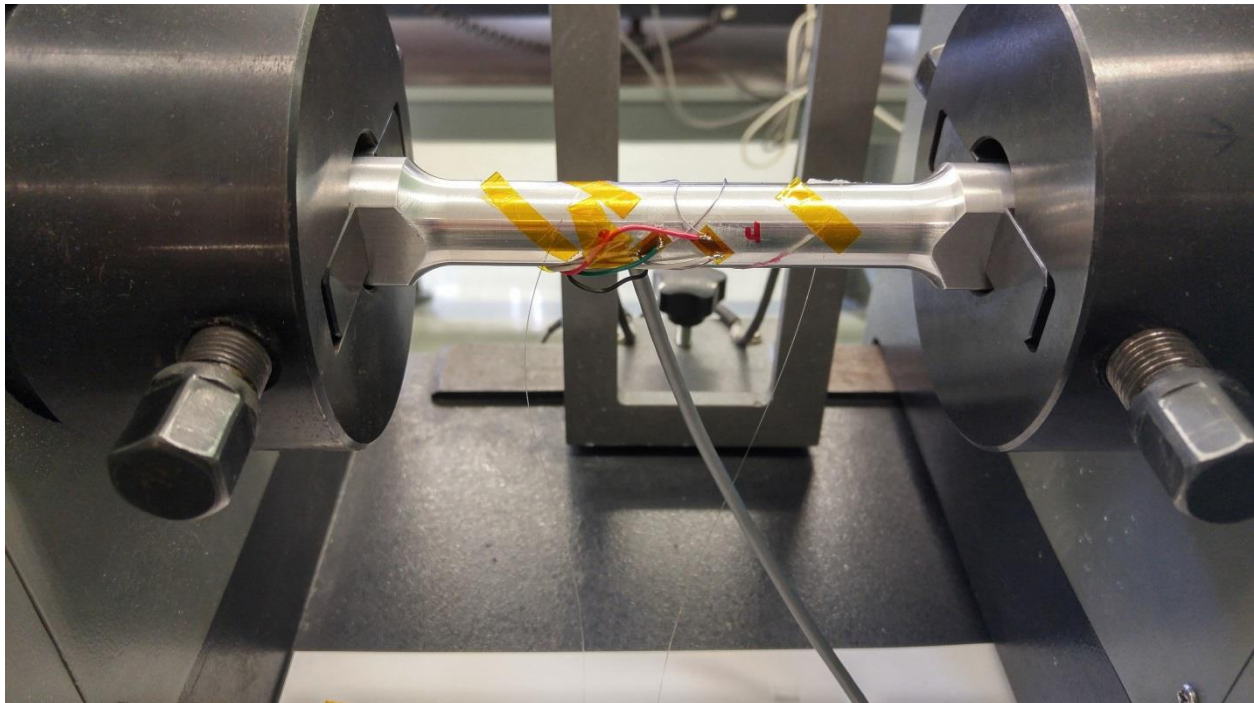

Figure 22 - Torsion rod with FBG-FP sensor and foil strain gauges bonded and held in the CTT202 Torsion Test machine.

3.2   Theoretical Calculations

Using the equations presented in section 2.5, the expected wavelength shift due to an applied torque was determined based on the geometry of the torsion rod used. Based on the material properties of aluminum 6061-T6, the theoretical torsion results are presented in Table 7.

Theoretical Torsion Results						
Torque (Nm)	Shear Stress (MPa)	Angular Deflection (radians)	με Fiber	Wavelength (pm)	Δλ (pm)	Δλ/N·m
10	6.385	0.006	123.563	149.39		
20	12.771	0.011	247.126	298.78	149.39	14.94
30	19.156	0.017	370.689	448.16	149.39	14.94
40	25.541	0.022	494.253	597.55	149.39	14.94
50	31.927	0.028	617.816	746.94	149.39	14.94
60	38.312	0.033	741.379	896.33	149.39	14.94
70	44.697	0.039	864.942	1045.71	149.39	14.94

Table 7 - Theoretical results to determine the wavelength shift experienced by the FBG-FP sensor due to the applied torque.

The critical value presented with these results is the wavelength shift due to the applied torque, Δλ/N·m = 14.94pm. As the PDH platform measures wavelength shift, it is critical for us to determine this parameter so that we can determine the applied torque to the shaft using the PDH measurement platform.

The same strain, as presented in Table 7, would be experienced by the foil strain gauges as they are bonded to the shaft at the same angle of 45°. The amplifier used provides an excitation voltage of 5V across the Wheatstone bridge, and has a gain of 1250V/V. The theoretical change in voltage across the Wheatstone bridge due to the applied torque is 8.51μV/N·m.

3.3   Torsion Rod FBG-FP Sensor Calibration

To ensure the wavelength shift of the FBG-FP sensor due to an applied torque is correct, a calibration was performed without using the PDH measurement platform. While mounted within the torsion machine, the FBG-FP sensor was monitored using the Agilent 8164A as known torques were applied to the shaft and held there while the measurement was taken. A peak of the Fabry-Perot cavity was monitored, and the wavelength shift was noted down for each new step in torque applied to the rod. Two runs were performed and the results are presented in Figure 23.
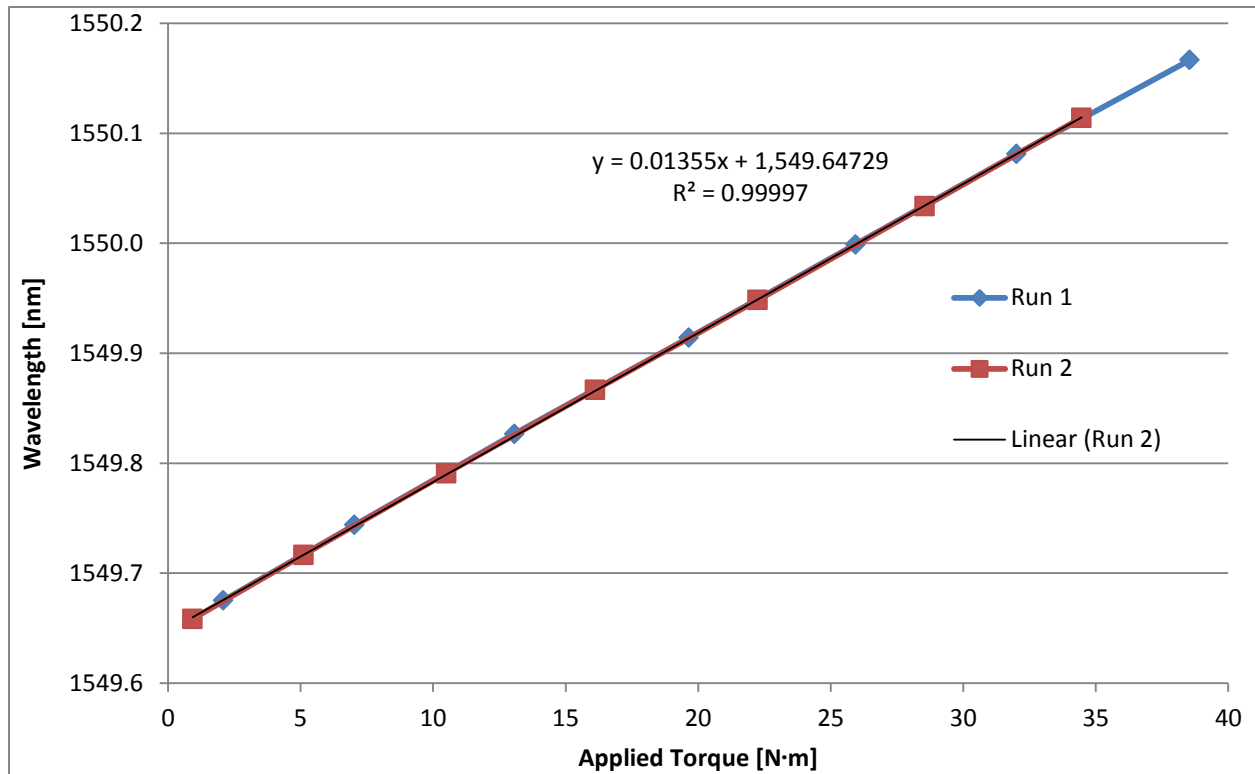
Figure 23 - Calibration results of the FBG-FP sensor using the Agilent 8164A.

The linearity of the sensor over the applied torque range from approximately 0N·m to 40N·m was excellent, as the R-squared value achieved was 0.99997. This was not unexpected, as this test is similar to the weight test previously perform; the FBG-FP sensors response is linear to an applied strain.

The slope of the line, however, was measured to be 13.5pm/N·m. This is an error of 10% from the theoretical value expected as presented in Table 7, which could be the result of a few causes. The first could be the wrap angle of the fiber optic sensor, as any shift away from 45° will result in a smaller torsion being measured due to the applied torque. The second source of error could be due to the tolerances of the material properties of the shaft. Although the material used was aircraft grade, tolerances were not provided by the manufacturer on critical material properties. The ASTM standard for 6061-T6 specifies the percentages of material required to make up the alloy, but it does not call for any tolerances to be specified about the alloy after manufacturing. The modulus of rigidity, for instance, does not have a tolerance from the manufacturer but could impact the calibration value significantly. The third source of error could be the strength of the bond between the fiber optic cable and the shaft. It was assumed, for simplicity, that this bond

was rigid, as cyanoacrylate materials typically are. Measurements were not performed to determine if this was the case for the bond formed during this experiment.

Overall, the results highlight a need to properly calibrate the wavelength shift due to an applied torque value, as it does deviate from the theoretical number determined. The deviation, and the cause for the deviation, is to be highlighted as future work for optimizing the torque sensor and ensuring the absolute accuracy of the torque value. Although the calibration completed here is not ideal and needs improvement, for the results presented in this work the value of 13.5pm/N·m will be used.

4. Experimental Results

Tests were performed by setting up test parameters in the control software of the CTT202 Torsion Test machine. The angular rate of change needed to be specified, which defined how quickly the torque was applied, and the end torque value needed to be set. An example of a run, with the results presented in Figure 26, is described in Table 8.

Step	Angular Rate of Applied Torque (°/min)	End Torque (N·m)
1	1	2.8
2	1	0
3	1	2.8
4	1	0
5	1	2.8
6	1	0
7	1	2.8
8	1	0
9	2	2.8
10	2	0
11	2	2.8
12	2	0
13	3	2.8
14	3	0
15	3	2.8
16	3	0
17	4	2.8
18	4	0
19	4	2.8
20	4	0
21	5	2.8
22	5	0
23	5	2.8
24	5	0
25	6	2.8
26	6	0
27	6	2.8
28	6	0

Table 8 - CTT202 Torsion Machine test profile defined.

The data for the torsion machine is logged by the manufacturer's software, and after the run can be exported as a text file. The data exported is not the raw sensor data from within the machine, but instead a filtered subset of it. The output contains approximately 16SPS.

The data for the optical sensor and the foil strain gauges was logged using LabVIEW on another computer, and was logged at measurement frequency of 10,000SPS. The raw data is recorded into a text file, and the data is then averaged over 20 samples to achieve a measurement frequency of 500SPS.

The full-scale measurement of the optical fiber on this shaft is quickly determined based on the maximum strain it can measure, 2328με. With a theoretical value of 12.36με/N·m, the full-scale torque the FBG-FP sensor can record is approximately 188N·m. As the platform is intended to demonstrate high accuracy, the testing performed was conducted over a small range of applied torque; 0N·m to 3N·m.

4.1 FBG-FP Experiment Results vs. Foil Strain Gauges

The first test conducted was a dynamic application of torque with a rate of change of 6°/min and is presented in Figure 24 with the data from all three sensors.

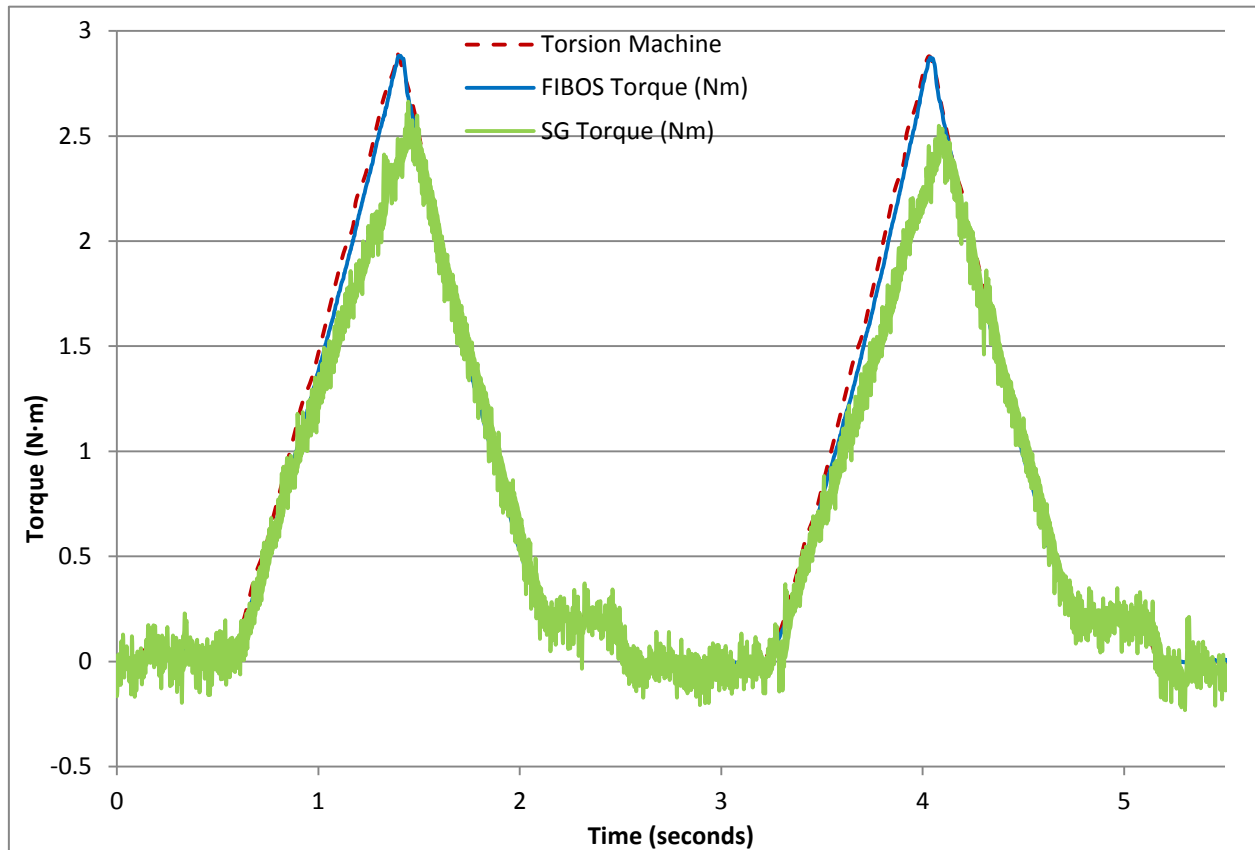**Figure 24 - Dynamic Torque run with a ramp speed of 6 °/min. The lines presented here are as follows: Red dashed line is the torsion machine data, the blue solid line is the FBG-FP torque, and the green line is the strain gauge data.**

It can be seen that the electrical noise present on the strain gauge impacts the minimum resolution, but that the overall shape does follow what the torsion machine is doing, as seen by the red dashed line. The strain gauge data, as can be seen at the peak torque value, appears to lag behind both the FBG-FP sensor and the torsion machine data. This was consistent for all measurements performed by the strain gauges, which would imply that the rate of change could not be accurately measured by the strain gauges. This could be a result of how the four foil gauges were bonded to the torsion rod, and would need to be explored further in order to better understand the deviation and lack of correlation to the torsion machine data.

The location of the four foil strain gauges to the electric motor within the torsion test machine likely had an impact on the noise measured, along with the location of the strain gauge amplifier. Attempts were made to reduce the noise; however eliminating the noise was not possible. For the remainder of the tests, an evaluation of just the FBG-FP sensor against the internal torque sensor within the torsion machine will be presented.
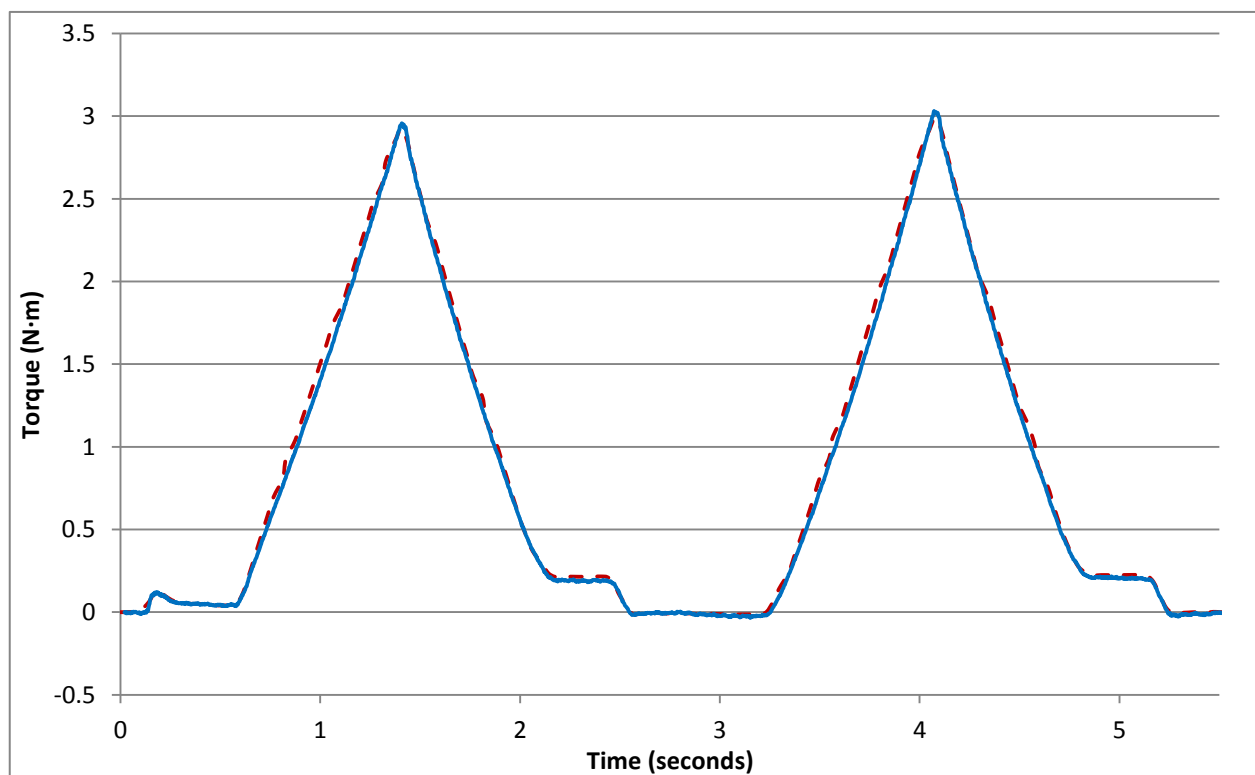

Figure 25 - Dynamic torque run with only the torsion machine data (red dashed line) and FBG-FP sensor data (blue line) shown.

4.2 FBG-FP Experiment Results vs. Torsion Test Machine Torque Sensor

Removing the strain gauge data, a better review of the performance of the FBG-FP sensor can be seen in Figure 25. The FBG-FP sensor tracks the change in torque well, matching the shape of the torsion machine data as torque is applied and removed. Utilizing the calibration value of 13.5pm/N·m for the FBG-FP sensor, and 4.3pm/mA for the laser diode within the measurement platform, the amplitude of the FBG-FP sensor measured above the torsion machine.

The average overshoot value was +0.7% of the torsion machine data and occurred when the machine reached the peak and minimum torque values; that is, when a change in direction was performed. To isolate the cause of the overshoot, and determine if the amount of overshoot was consistent, a test was conducted that varied the rate of change during a single run. The angular rate of change was varied from 1°/min to 6°/min, with 1° increments. The results are presented in Figure 26, and show an interesting trend. Throughout the test, the FBG-FP sensor continues to follow the correct shape; however the peak amplitude continues to be higher than that which was measured by the torsion test machine.
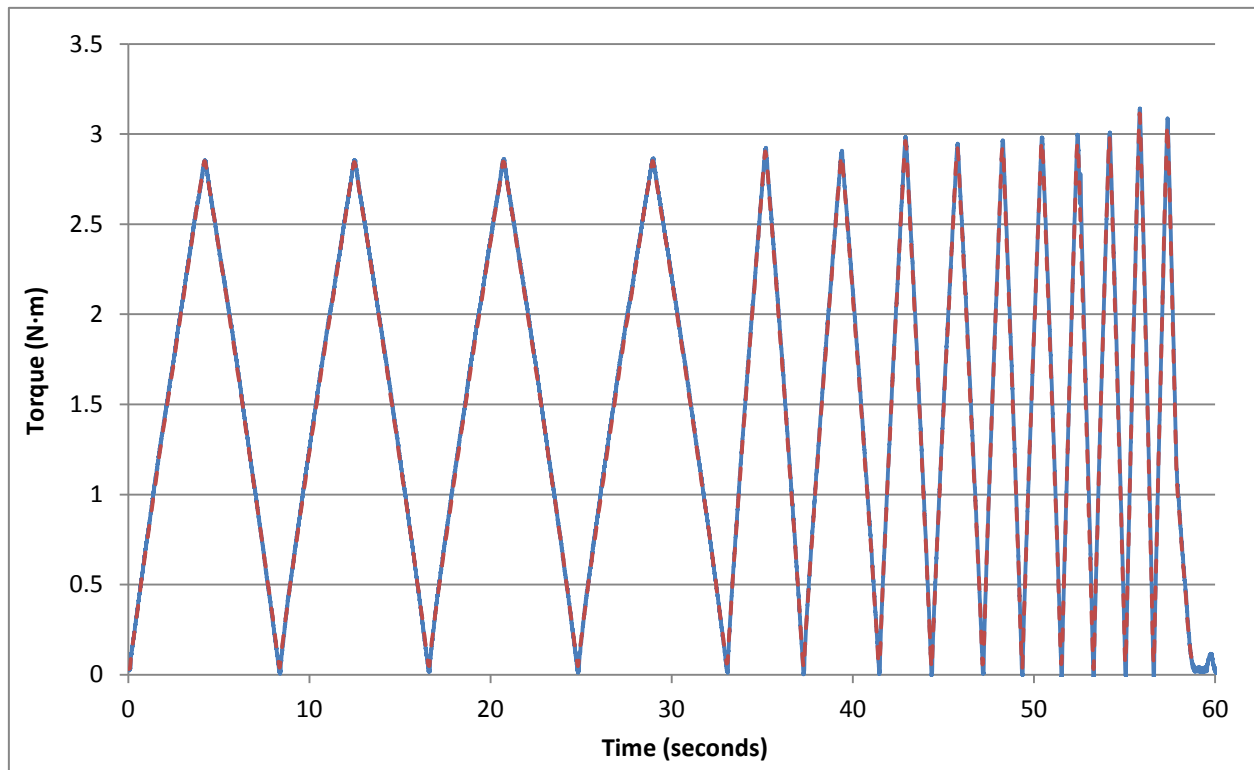

Figure 26 - Dynamic torque run with varying ramp speeds; from 1°/min to 6°/min. Torsion machine data (red dashed line) and FBG-FP sensor data (blue line) shown.
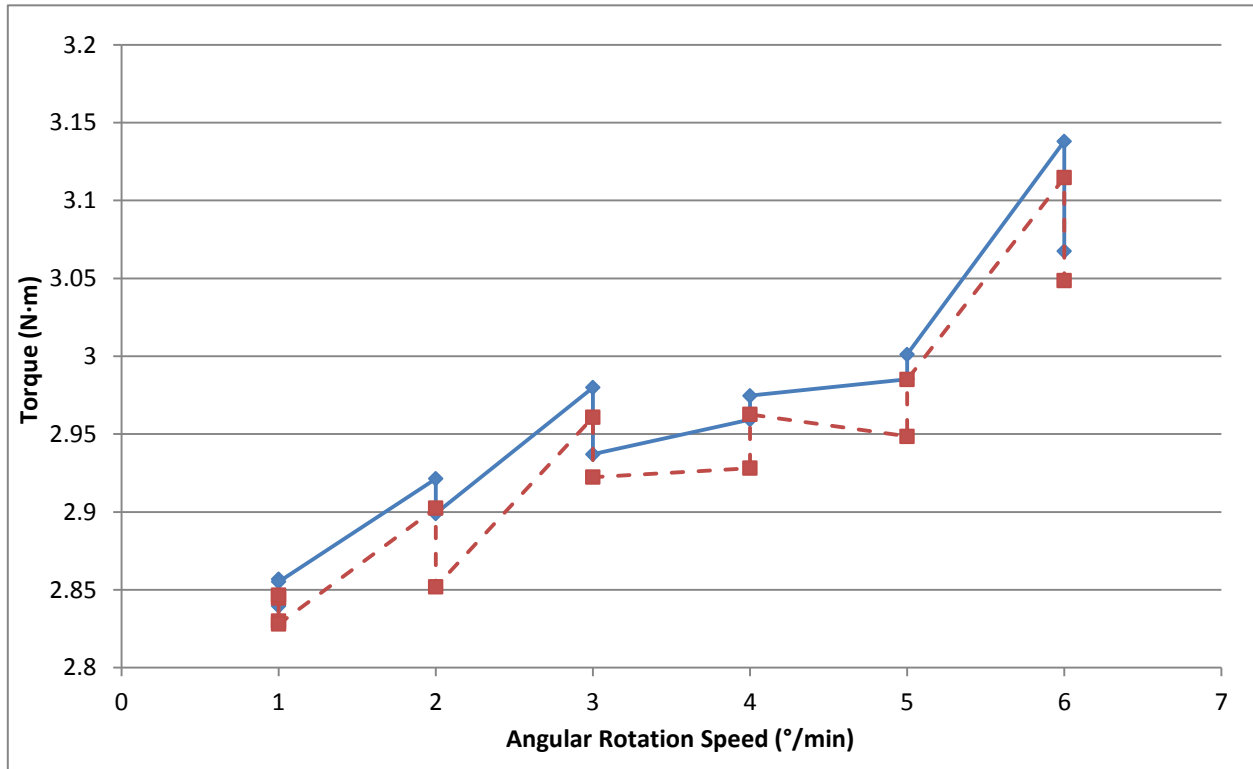
Figure 27 - Comparison of peak torque measured during dynamic torque run with varying ramp speeds; from 1°/min to 6°/min. Torsion machine data (red dashed line) and FBG-FP sensor data (blue line) shown.

The difference in the amplitudes of the peak torque measured during each cycle averaged +0.7%, with a variance of +/-0.9% across the 14 peaks. It is also of interest that as the rate of change increases, the torsion machine is no longer capable of hitting the set end torque value of 2.8N·m, and instead begins to overshoot the desired setpoint. This is likely due to the machine being unable to slow down the rotating mass, and at the highest rate selected, 6°/min, we saw an overshoot of 0.311N·m from the desired end torque value. This trend is seen in both the torsion machine's data, along with the FBG-FP sensor, as presented in Figure 27. This demonstrated that the error seen in the FBG-FP sensors data was not due to the rate of change of torque, but could perhaps be demonstrating that the FBG-FP sensor is measuring a more exact value of torque during these quick rate changes. Further research needs to be performed to explore these results.

After dynamic tests were performed, the performance of the sensor under a static applied torque was demonstrated. In this test, torque was applied to approximately 2.8N·m, and held for a period of 30 seconds. The torque was removed for a short period of time, then re-applied for another 30 seconds. The results of FBG-FP sensor can be seen against the torsion machine data in Figure 28.

40
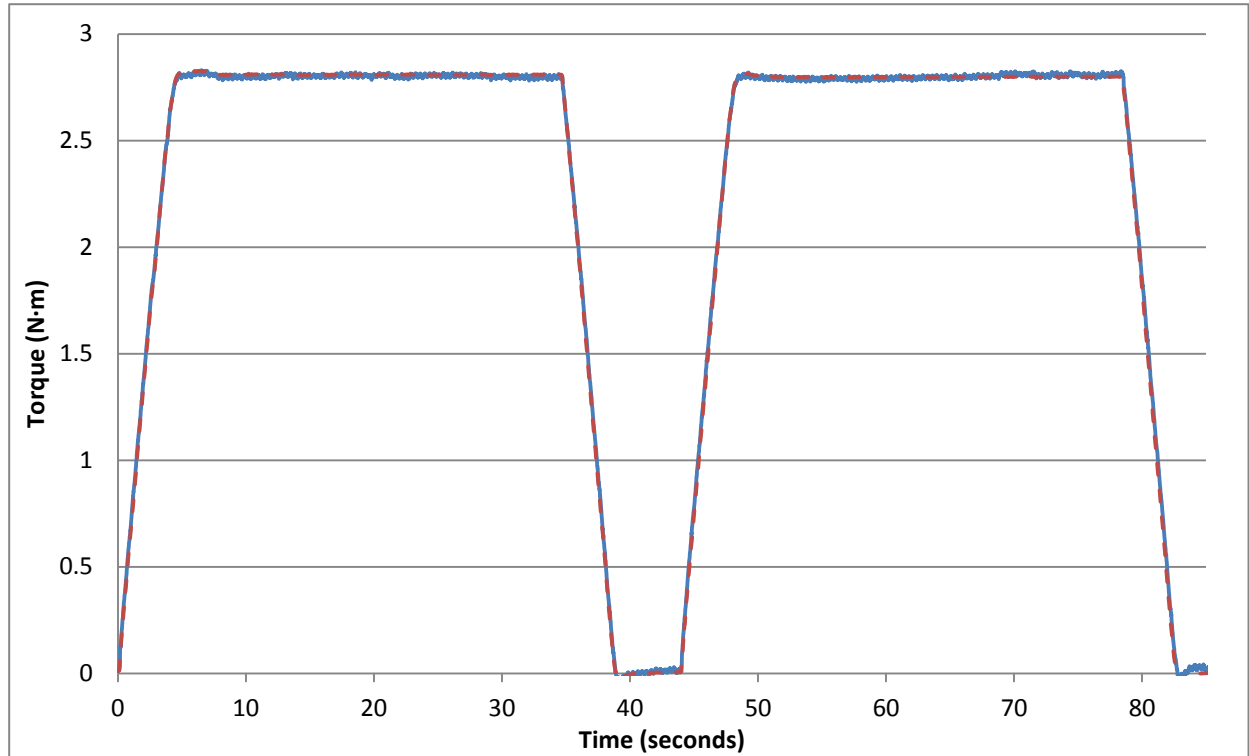
Figure 28 - Ramp and hold torque for approximately 30 seconds. Torsion machine data (red dashed line) and FBG-FP sensor data (blue line) shown.

The error between the two sensors was less than 1% while being held at a known torque, which was similar to the error measured in the dynamic results. A more appreciable error was seen towards the end of the test, around 70 seconds in, when the FBG-FP sensor begins to deviate from the held torque value. As the torsion machine does not show this change, it is believed that a temperature change may have occurred at the sensor.

As the sensor is bonded to aluminum, with a thermal coefficient of expansion of approximately 23μm/°C, the sensor will experience a wavelength shift of approximately 27pm for every 1°C of temperature change. As the temperature of the specimen was not monitored, it cannot be confirmed but it is strongly suspected to be the cause of the drift seen in Figure 28.

41

5. Conclusions and Future Work

5.1 Conclusions

A measurement platform capable of showcasing the possible advantages of optical sensors over foil strain gauges was demonstrated. Measurements performed show the platform achieving high measurement resolution for torsion and high strain accuracy against the Agilent 8164A. This was achieved while providing high bandwidth for continuous measurements. The cost of the unit developed also met the desired target, with a bill of materials cost of approximately $2,000 with the possibility to further reduce the price in production volumes.

Compared against the torsion test machine, a small measurement error of up to 1.65% was seen in the absolute torque value recorded. This difference, although quite small, needs to be further explored to understand which measurement device is reading the absolute value accurately. Overall, the measurements made by the FBG-FP sensor do successfully follow along well with the applied torque measured by the torsion machine.

The calibration procedure for the FBG-FP sensor and PDH measurement platform used during this experiment relied on two external devices; the torsion test machine and the Agilent 8164A. By monitoring the wavelength shift of the FBG-FP sensor with the Agilent 8164A and applying a known torque with the torsion machine, a calibration value of 13.5pm/N·m was determined. The issue with this method is that the measurement accuracy of the Agilent 8164A and the accuracy of torque set by the torsion machine must be accounted for. The torsion machine manufacturer does not provide a calibration procedure for the machine, or information on how it was calibrated at the factory. As a result, it is difficult to determine the accuracy of the torque value it produces through the rotation of the shaft, and the accuracy of the torque data measured by the internal torque sensor. Instead, we need to rely on the datasheet provided by the manufacturer that specifies a indicated torque accuracy of +/-1%; a value very close to the error that was measured between the FBG-FP sensor and the torsion machine.

An ideal calibration procedure for the PDH measurement platform would be to copy what is done already for commercially available sensors. The calibration method used for torque sensors today involves fixing one end of the torque sensor, and attaching a torque arm to the other end.

On this torque arm, calibrated weights are used to apply a known torque to the sensor. This could be done for the PDH measurement platform and FBG-FP sensor if a fixture was built to do so.

Although the absolute torque value may be incorrect by upwards of 1.65%, the resolution achieved by the platform can still be determined by evaluating the noise presented in the raw data gathered in Section 4. While the sensor was being held at 2.8N·m, there was the equivalent of +/-0.0271N·m of noise present. With the full scale torque measurement set to 188N·m, the noise on the signal represents a minimum measurement resolution of +/-0.015% of FS torque. This is below that of the HBM T12 sensor introduced earlier, which publishes a resolution of only +/-0.05% of FS torque, and shows the possibility of creating a fiber optic torque sensor that can compete with one of the industry's best available sensors.

In terms of the wavelength shift, the minimum detectable wavelength shift measured is based off the noise measurement of +/-0.0271N·m, and translates to +/-0.36pm. The minimum detectable strain measured is +/-0.335με; very close to the theoretical value of +/-0.233με as presented in Section 2.3.2.

The platform requirements also specified a system that needs to be a low cost optical solution and comparable in cost to commercially available foil strain gauge amplifiers. With a full cost breakdown presented in Appendix B, through the development of custom hardware, a solution cost of $2,000 was achieved. In volume, pricing of all the components would see a drop in price, and with a re-design for cost reduction, the solution cost could fall under $1,000. The sensor cost is not highlighted here as they were not purchased during this testing, but manufactured at Ryerson. In production, the sensor cost would fall between $50 to $150 depending on the coating material selected (i.e. polyimide, acrylate or bare glass).

Overall, this was a successful demonstration of a high measurement bandwidth, high accuracy and low cost fiber optic sensor measurement platform.

5.2   Future Work

In order to ensure the accuracy of the torque measurement, future work must revolve around developing a calibration fixture to properly calibrate the PDH measurement platform and the FBG-FP sensor. Once the absolute torque value is known to be correct, rotational torque

measurements should be explored. The testing performed in this body of work was done on a reactionary fixture, where one end of the rod was fixed and the other end was rotated. In future work, the FBG-FP sensor should be mounted to a rotating shaft through an optical rotary joint and torque measurements should be performed and compared against commercially available sensors. This future work can begin to evaluate the benefits of removing an in-line torque sensor, and improvements in the torque measurements can be seen through the reduction of rotating mass with the number of couplers required. In addition to evaluating rotating torque, the effects of temperature should be reviewed and adjusted for. The FBG-FP does experience a wavelength shift due to a change in temperature, and therefore temperature needs to be monitored in order to factor out the effects of it.

With regards to just the PDH measurement platform, future work needs to revolve around the design and development of a high-speed photodiode receiver. The PID speed can also be further improved by moving away from an embedded processor, and instead utilizing a FPGA to handle the RF modulation and PID control loop. This would not only have a positive impact on the performance of the system, but could also be a source of cost reduction for the overall platform.

Appendix A
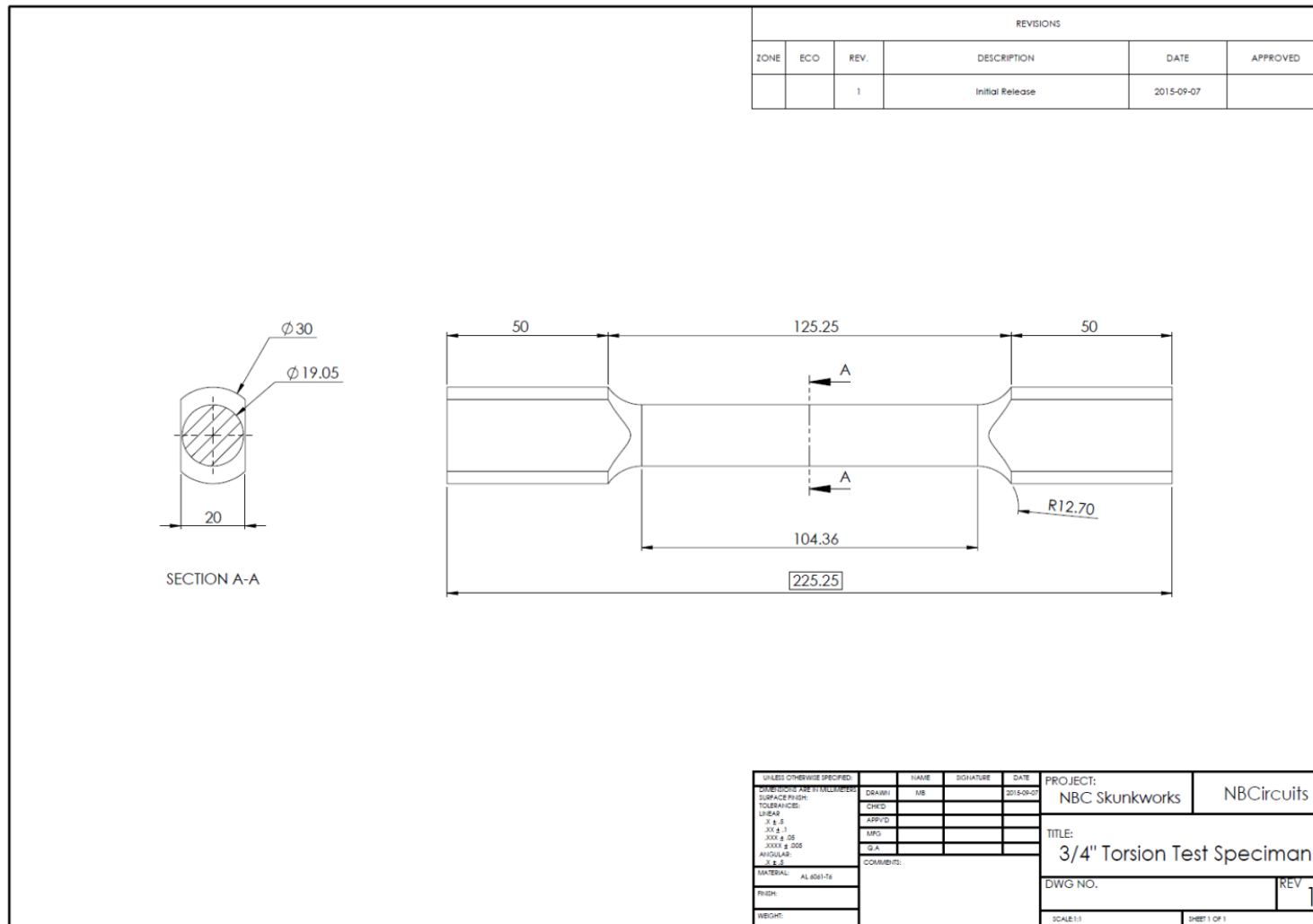
Appendix B

PDH Measurement Platform Bill of Materials			
Description	Cost per unit	Total Quantity	Total Cost
Raspberry Pi 3	$ 60.00	1	$ 60.00
1U Server Case + Machining for cut-outs	$ 252.06	1	$ 252.06
Power Switch - Green	$ 21.74	1	$ 21.74
Panel Power Connector	$ 5.28	1	$ 5.28
Power Harness Connector	$ 3.33	1	$ 3.33
Power Harness Mounting Hardware	$ 0.39	1	$ 0.39
Power Supply - Wall Adapter - 24V @ 1A	$ 23.83	1	$ 23.83
FC/APC to FC/APC Panel Mount Connector	$ 3.75	1	$ 3.75
3-port 1.55um Optical Circulator	$ 183.00	1	$ 183.00
150MM SMA to SMA cable	$ 10.50	2	$ 21.00
100MM SMA to SMA cable	$ 10.00	1	$ 10.00
DFB 14-pin Butterfly	$ 180.00	1	$ 180.00
Photodiode Board (PCB + component cost + assembly cost)	$ 200.00	1	$ 200.00
RF Board (PCB + component cost + assembly cost)	$ 301.09	1	$ 301.09
Laser Control Board (PCB + component cost + assembly cost)	$ 675.98	1	$ 675.98

Total	$ 1,941.45

References

[1] Persistence Market Research, "Global Market Study on Torque Sensor: Rotary Torque Sensor Expected To Be the Most Valuable Product Type Segment throughout the Forecast Period," New York City, 2015.

[2] S. Rajaram, "Global Markets and Technologies for Sensors," BCC Research, Wellesly, February 2016.

[3] P. K. Stein, "Strain Gauge History and the end of the twentieth century," *Experimental Techniques,* pp. 15, 16, 2001.

[4] A. D. Kersey, M. A. Davis, H. J. Patrick, M. LeBlanc, K. Koo, C. G. Askins, M. A. Putnam and E. J. Friebele, "Fiber Grating Sensors," *Lightwave Technology,* vol. 15, no. 8, pp. 1442-1463, 1997.

[5] B. Culshaw, "Optical Fiber Sensor Technologies: Opportunities and - Perhaps - Pitfalls," *Lightwave Technology,* vol. 22, no. 1, pp. 39-50, 2004.

[6] Omega Engineering, "The Strain Gage," [Online]. Available: http://www.omega.ca/literature/transactions/volume3/strain.html. [Accessed 20 June 2016].

[7] HBM T12 Datasheet, "HBM T12," [Online]. Available: https://www.hbm.com/en/2377/t12-innovative-ultra-high-precision-digital-torque-transducer/. [Accessed 30 June 2016].

[8] K. O. Hill and G. Meltz, "Fiber Bragg Grating Technology Fundamentals and Overview," *Lightwave Technology,* vol. 15, no. 8, pp. 1263-1276, 1997.

[9] X. G. Tian and X. M. Tao, "Torsion Measurement Using Fiber Bragg Grating Sensors," *Experimental Mechanics,* vol. 41, no. 3, pp. 248-253, 2001.

[10] P. L. Swart, A. A. Chtcherbakov and A. J. van Wyk, "Dual Bragg grating sensor for concurrent torsion and temperature measurement," *Measurement Science and Technology,*

vol. 17, pp. 1057-1064, 2006.

[11] L. W. Cornett, "Fiber Optic Sensors: Global Markets," BCC Research, Wellesley, 2014.

[12] E. D. Black, "An introduction to Pound–Drever–Hall laser frequency stabilization," *American Journal of Physics,* vol. 69, no. 1, pp. 79-87, 2001.

[13] R. Gafsi and M. A. El-Sherif, "Analysis of Induced-Birefringence Effects on Fiber Bragg Gratings," *Optical Fiber Technology,* vol. 6, pp. 299-323, 2000.

[14] P. Antunes, F. Domingues, M. Granada and P. Andre, "Mechanical Properties of Optical Fibers," in *Selected Topics on Optical Fiber Technology*, InTech, Available from: http://www.intechopen.com/books/selected-topics-on-optical-fiber-technology/mechanical-properties-of-optical-fibers, 2012, pp. 537-550.

[15] ASTM International, "ASTM E143-13, Standard Test Method for Shear Modulus at Room Temperature," West Conshohocken, PA, 2013.

[16] C. Voigtländer, R. G. Becker, J. Thomas, D. Richter, A. Singh, A. Tünnermann and S. Nolte, "Ultrashort pulse inscription of tailored fiber Bragg gratings with a phase mask and a deformed wavefront [Invited]," *Optical Materials Express,* vol. 1, pp. 633-642, 2011.

[17] R. Schicker and G. Wegener, "Measuring Torque Correctly," [Online]. Available: www.hbm.com. [Accessed 20 July 2016].